ARL-STRUC-R-448

AR-007-070

DEPARTMENT OF DEFENCE

DEFENCE SCIENCE AND TECHNOLOGY ORGANISATION

AERONAUTICAL RESEARCH LABORATORY

MELBOURNE, VICTORIA

Aircraft Structures Report 448

DESIGNING FOR DAMAGE TOLERANT COMPOSITE REPAIRS

by

W.K. CHIU
D. REES
P. CHALKLEY
R. JONES

Approved for public release.

OCTOBER 1992

DISCLAIMER NOTICE

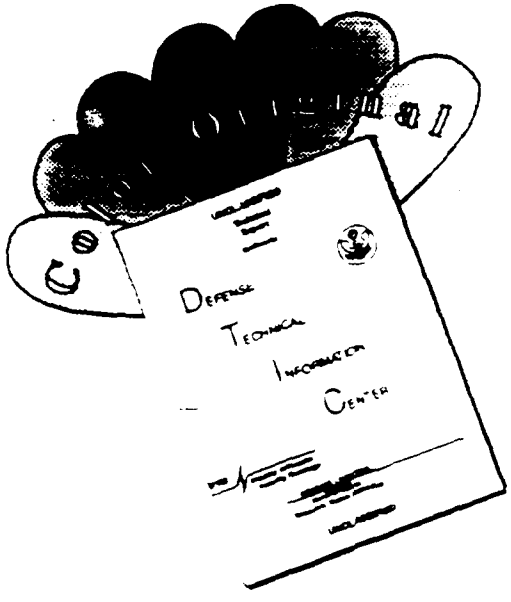

THIS DOCUMENT IS BEST QUALITY AVAILABLE. THE COPY FURNISHED TO DTIC CONTAINED A SIGNIFICANT NUMBER OF COLOR PAGES WHICH DO NOT REPRODUCE LEGIBLY ON BLACK AND WHITE MICROFICHE.

AR-007-070

DEPARTMENT OF DEFENCE
DEFENCE SCIENCE AND TECHNOLOGY ORGANISATION
AERONAUTICAL RESEARCH LABORATORY

Aircraft Structures Report 448

DESIGNING FOR DAMAGE TOLERANT COMPOSITE REPAIRS

by

W.K. CHIU
D. REES
P. CHALKLEY
R. JONES

SUMMARY

This paper presents a design methodology, and the associated data base, for the damage tolerant design of adhesively bonded repairs. This methodology is illustrated by considering repairs to an edge cracked panel and to multi-site damage in a fuselage lap joint.

POSTAL ADDRESS: **Director, Aeronautical Research Laboratory**
506 Lorimer Street, Fishermens Bend 3207
Victoria Australia

CONTENTS

1. INTRODUCTION

Externally bonded composite patches are an effective method of repairing cracked, or damaged, structural components, [1]. Whilst this repair methodology was first used to repair cracks in military aircraft it has recently been applied to civilian aircraft. An application to Boeing 727 and 747 aircraft is described in [2,3], which outline a series of flight demonstrator programs, whilst a repair to the keel beam of a Boeing 767 aircraft is described in [4]. In 1990, with the support of the Australian Civil Aviation Authority (CAA), a world wide study into the commercial application of this technology was performed, see [5]. Thirty four organisations in eight countries, including ten manufacturers and seven regulatory authorities were consulted. The following proposed design rules and procedures were subsequently adopted by the CAA; viz:

1) Designs shall be substantiated against the Damage Tolerance provisions of the United States Federal Aviation Regulations (FAR) Part 25.571 at Amendment 45 or equivalent JAR 25.571.

2) The repair of any structural component which contains damage sufficient to reduce the aircraft structure to below design limit load residual strength shall not normally be attempted.

3) Service time degradation, environmental and impact damage substantiation evidence shall be provided for the composite material and the structural bond, as appropriate to the design. This should include sufficient work to enable the composite repair to meet the intent of the damage tolerance requirements.

4) Quality control consideration should include, for all critical areas, wedge testing of bond strips produced during the repair process.

The purpose of this report is to discuss a design methodology, and the associated design data base, for the damage tolerant design of composite repairs to cracked metallic structural components. This approach will be illustrated by considering the repair to an edge cracked panel and to multi-site damage (MSD) in a fuselage lap joint. In this case attention will focus on the externally bonded repair described in [2,3,4,6].

In the CAA Airworthiness Advisory Circular it was stated that

".....civil requirements do not mandate an initial flaw approach. However, it is often convenient to do so and this may reduce the threshold fatigue testing requirement. This may be in recognition of leaving the initial crack in the metal unchanged but also may cover the presence of an unbonded region in the joint."

In light of these comments the current fatigue test programs, discussed in this report, have included cracks, in each of the test specimens, and the associated repairs have in-built disbonds and/or impact damage.

When designing bonded repairs, or adhesively bonded joints, the stress/strain response of the adhesive plays a central role in determining both the load carrying

capacity and the fatigue performance of the repair or joint, see [7-9]. To date FM73, which can be cured at 80°C, is the adhesive most commonly used for bonded repairs, see [1]. This report presents the stress/strain response for this particular adhesive, determined using a thick adherend test specimen [10], at various strain rates. An analytical representation for this rate dependent stress/strain response is also presented.

2. ADHESIVE DESIGN ALLOWABLES

The research undertaken as part of the Primary Adhesively Bonded Technology (PABST) program [7] revealed that adhesively bonded structures are significantly more tolerant to large disbonds than had previously been thought. The PABST fuselage was made using "development" tooling and contained a number of significant flaws. These flaws did not grow during testing [8]. Similarly, the environmental fatigue testing of representative coupons did not damage the adhesive bonds [8]. This test program led to the widespread acceptance of several simple formulae for calculating the maximum load carrying capacity of a bonded joint. For a symmetrical joint subjected to a uniform remote tensile stress the maximum load P, that can be carried by the bond, is given, see [9], by the formulae;

$$P = 2\sqrt{tWET} \qquad (1)$$

where E is the Youngs modulus of the adherend , W is the maximum permissible value of the strain energy density of the adhesive, whilst t and T are the thicknesses of the adhesive and the adherend respectively. Here W can be determined experimentally using the thick adherend test specimen.

For bonded structures the PABST program also revealed that, for thin skinned structures, the use of da/dn calculations, to life a bonded joint, is inappropriate and, in some instances, potentially detrimental, see [8]. For such structures the bond (joint) can always be designed such that damage will not initiate. Furthermore, if the bond is found to contain damage, i.e. delaminations or disbonds, then this damage will not grow, even under adverse environmental conditions, see [6,8]. In this case the joint should be designed such that the stresses and strains in the adhesive are beneath a limiting value, which we will term the "threshold" value, for the particular adhesive. (It should be noted that for cracks in thin skins an externally bonded repair can always be designed such that; 1) the crack does not grow, and 2) the maximum permissible strain in the repair is not exceeded. A more detailed discussion of these design criteria is given in [1,6].)

For a given symmetrical joint, with a fixed adhesive and adherend thickness, the "fatigue threshold" load P_f below which irreversible damage in the adhesive will not occur can be calculated, as in equation (1), from the formulae;

$$P_f = 2\sqrt{tW_fET} \qquad (2)$$

where W_f is the "threshold" value of the strain energy density of the adhesive, i.e. the value below which irreversible effects will not occur. The value of W_f can be

determined experimentally using the thick adherend test specimen. For aerospace applications P should be beneath ultimate load for the component and the value of P_f should be beneath limit load.

To minimize the thermal mismatch problem for boron epoxy repairs to thin metallic skins it is best to use an adhesive which can be cured at the lowest possible temperature. As a result the thin film adhesive FM73, which can be cured at 80°C, is extensively used for bonded repairs. Section 2.1 will present the stress/strain response of this particular adhesive, determined using the thick adherend test specimen, for various strain rates, together with the associated values of W_f. An analytical representation for this rate dependent stress/strain response, which is capable of reproducing the observed irreversible effects, will then be presented. An extension of this work, to account for environment effects, will be presented in a subsequent report.

The advantage of expressing the "fatigue threshold" load P_f in terms of the quantity W_f, rather than the associated stress or strain threshold values, is purely due to computational considerations. This aspect will be discussed in Section 3.1.

2.1 Rate Dependent Response of FM73 Thin Film Adhesive

As has been mentioned in Section 2 the stress/strain behaviour of the adhesive plays a central role in determining both the load carrying capacity and the fatigue performance of a bonded repair. This section presents the stress/strain response of the commonly used adhesive FM73, obtained using a thick adherend test specimen, at various strain rates. An analytical representation for this rate dependent stress/strain response will be presented in Section 2.2.

2.1.1 Specimen Preparation

The results presented in this section were obtained using the symmetric, thick adherend, short overlap, shear test specimen. The dimensions of the lap shear specimen are shown in Figure 1. These specimens were made from hardened tool steel.

The bond surfaces of the specimen, after being grit blasted, were immersed in a 1.0% silane solution for about 10 mins. They were then dried in an oven at 80°C. The dried specimens were subsequently assembled with a FM73 film adhesive at room temperature. These assembled specimens were then vacuum bagged and placed in an autoclave where the adhesive was cured under a pressure of 105 kPa and at a temperature of 120°C. The bond line thickness of this joint was approximately 0.2 mm (i.e. this is a typical adhesive thickness for 1 layer of FM73).

2.1.2 Experimental Method

The specimens were loaded under strain control, in a 10kN Instron test machine and the shear strain was measured using a pair of linear variable displacement transducers (LVDT). A clip gauge was attached to the LVDT to provide a feedback signal for the

control unit in the Instron. This clip-gauge was necessary because the control signal from the LVDT was too noisy for the Instron control circuit.

The load cell, LVDT's and the clip gauge were calibrated prior to each experiment. Readings from the LVDT and the load cell were acquired using an IBM Personal Computer. The sampling frequency of the acquisition unit was varied according to the strain rates used in each experiment.

The results presented in this paper were obtained from a set of experiments performed at room temperature. The nominal temperature in the test laboratory was approximately 19^{o}C.

It is known that the stress distribution in the adhesive layer of the lap shear joint is complex, especially around the corner of the joint. The material discontinuity (i.e. at the adhesive and steel adherend interface) results in a region of high peel stress. This region of high stress, although highly localised, is a potential failure location. To avoid failure, the experiments were usually terminated at a shear strain of 0.4.

2.1.3 Experimental Results

The experiments were conducted at four strain rates, 8.80e-2, 8.67e-3, 8.78e-4 and 8.68e-5 /sec. Prior to the experiments used to characterise the FM73, a set of initial tests were performed to test repeatability. Figure 2 shows these initial test results for a strain rate of 8.78e-4 /sec. The deviation in the results is in the order of 5%, which can be attributed to various sources of experimental error.

Figure 3 shows various stress-strain curves obtained at different strain rates. These diagrams reveal that the FM73 adhesive is strain-rate dependent, even at room temperature, (i.e. well below its glass transition temperature). It should be noted that it was difficult to control the test at the slowest strain rate. This was the result of endeavouring to control the experiment at a strain rate close to the lower limit of the machine, in terms of cross-head speed. The yield stresses tabulated in Table 1 are calculated from the experimental data using Consideres' construction [12]. This Table also shows a consistent value of the shear modulus obtained from this set of experiments.

Since the yield stress of the adhesive is dependent on the strain rate, it follows that the adhesive properties must have a strong dependence on time. One method of revealing this time dependency, is via a stress-relaxation test (i.e. strain hold test). Figure 4 shows the result of loading the specimen past yield at a particular strain-rate and then holding the strain at a constant value. This figure reveals a very large stress drop, to its "threshold" value, as a result of the strain hold. Figure 5 shows the stress-time relationship during the strain hold. The stress drop is initially exponential and then decays to a "threshold" limit. Figures 6(a) and 6 (b) show the results of stress relaxation tests at strain rates of 8.80e-2 and 8.67e-3 /sec respectively. The level of the stress relaxation seen in these figures reveals that the "threshold" to which the stress relaxes is independent of the value of the plastic strain, see [11]. The threshold value is also independent of the strain rate.

The stress overshoot that occurs on reloading the specimen after stress-relaxation (Figure 6) has been observed before in the thermoplastic, PVC, and was attributed to orientation hardening [12]. It is not clear whether the same mechanism would operate in a cross-linked polymer, except possibly at low cross-link densities characteristic of a rubbery state [12]. Regardless of the mechanism, however, the stress drop during stress-relaxation to its "threshold" value results in a conversion of elastic strain into inelastic strain, with the total strain remaining constant. This results in recoverable (i.e. elastic) strain energy being converted into irreversible energy, and as such is a direct reflection of the degradation of the adhesive. This degradation can be avoided by designing such that the adhesive stresses are beneath the "threshold" value. In this case irreversible damage will not occur. For the adhesive under consideration this "threshold" stress is approximately 25 MPa, which corresponds to a "threshold" energy W_f of 0.416 MPa. As can be seen from Table 1 the "threshold" stress corresponds to the lower limit of the yield (shear) stress, i.e. the value of the yield (shear) stress at vanishingly small strain rates.

TABLE 1: YIELD SHEAR STRESS AND ELASTIC SHEAR MODULUS AT VARIOUS STRAIN RATES

Strain Rate (/sec)	Yield Stress (MPa)	Shear Modulus (MPa)
8.68e-5	26.78	753
8.78e-4	32.81	746
8.67e-3	35.94	766
8.80e-2	39.06	758

2.2 Analytical Representation

A constitutive model was used to describe the behaviour of this adhesive. The model chosen is an extension of that developed by Ramaswamy [14], to describe the behaviour of Rene 80 at high temperatures. (The general behaviour of the adhesive under the monotonic tests described above in some respect resembles that of Rene 80 which exhibits extensive viscoplastic behaviour.) This constitutive model is based on state variables and therefore, it is not appropriate to define a yield surface. Since viscoplastic behaviour is analogous to viscous flow, it was envisaged that the post-yield macroscopic time dependent characteristics may be similar.

The model assumes that the inelastic strain rate is proportional to the "over-stress". This "over-stress" is the difference between the applied stress and the "back" stress that is built up within the material, viz.,

$$\bar{\sigma}_{ij} = \sigma_{ij} - \Omega_{ij} \tag{3}$$

where σ_{ij}, $\bar{\sigma}_{ij}$, and Ω_{ij} are the deviatoric components of the applied stress, the overstress stress and the back stress respectively. With this notation, the inelastic strain rate, $\dot{\varepsilon}_{ij}^{I}$ is expressed as,

$$\dot{\varepsilon}_{ij}^{I} = \sqrt{2}\, D \exp\left(\frac{-A}{2}\left(\frac{Z^2}{1.5|\bar{\sigma}_{ij}|^2}\right)^n\right)\left(\frac{\bar{\sigma}_{ij}}{|\bar{\sigma}_{ij}|}\right) \tag{4}$$

where A, D and n are constants to be determined experimentally. Z relates to the accumulation of inelastic work. Similar exponential relationships have been used in other unified theories to describe the constitutive behaviour of the time dependent inelastic strain of metals and thermoplastics (e.g. [11] and [15]). The "evolution" equation for the back-stress is shown in equation (5).

$$\dot{\Omega}_{ij}^{I} = f_1\, \dot{\varepsilon}_{ij}^{I} - 1.5 f_1 \left(\frac{\Omega_{ij}}{\Omega_s}\right)\dot{\varepsilon}_{ij}^{I} + f_2 \dot{\bar{\sigma}}_{ij} \tag{5}$$

where f_1 and f_2 are constants determined experimentally, Ω_s and $\dot{\varepsilon}_e$ are the saturated value of the back stress and effective inelastic strain rate respectively. The effect of the back stress is evident in Figures 6 (a) and (b). These figures show that when the applied load was removed, a reverse anelastic flow was observed.

Strain hardening is apparent in FM73 at large deformations (see Figure 2) and during re-loading following stress-relaxation (Figure 6). The mechanism for this strain hardening is unclear. It will be assumed that this hardening effect is a function of accumulated inelastic work [14]. The associated state variable, Z, is assumed to satisfy the following relation,

$$\dot{Z} = m|Z_1 - Z|\, \dot{W}^{I} \tag{6}$$

where m is a constant determined experimentally, Z_1 is the final value of the work hardening parameter which is determined experimentally and W^I is the plastic work. The constants for this model were determined using Singular Value Decomposition, which is essentially a least-squares fit. The shear stress/strain curve for the strain rate of 8.80e-2 /sec was predicted using the experimental results for strain rates of 8.68e-5, 8.78e-4 and 8.67e-3 /sec as input data. Figure 7(a), (b) and (c) shows the comparison between the experimental and the predicted curves. There is good agreement between the experimental and the theoretical results.

To further validate the constitutive model, a comparison with the stress relaxation experiments was made. Figure 8(a) and (b) show good agreement between the predicted and the experimentally obtained shear stress-strain relationship, including the value of the "threshold" stress. The magnitude of the overshoot, attributed to strain hardening of the polymer during reloading, is predicted quite well. However, the initial shape of the stress-strain curve during reloading differs somewhat from that predicted. Additional work is required to accurately represent this effect.

Figure 9 shows the comparison between the experimental and predicted stress-time relationship during a strain-hold (i.e., stress-relaxation experiment). The agreement between the experimental and predicted values is quite good and illustrates the ability of the model to describe the constitutive behaviour of this particular adhesive.

2.3 Discussion

The monotonic lap shear tests have quantified the strain rate dependency of FM73 at both room temperature and at elevated temperature. The stress-relaxation resulting from a strain hold was significant and reveals the "threshold" stress, below which irreversible effects do not occur. This "threshold" value is independent of strain rate and of the degree of plastic deformation. The extensive stress-relaxation, which occurs in a matter of seconds or minutes, can severely degrade the performance of the adhesive. This degradation is due to the conversion of recoverable elastic energy to irreversible inelastic energy, and can be avoided by designing such that the stresses (energy) are below the "threshold" value.

This report also presents an analytical model for the time-dependent inelastic deformation of the adhesive.

3. DESIGNING FOR DAMAGE TOLERANT BONDED JOINTS

There are several methods available for designing composite repairs to cracks in thin metallic skins, i.e. typical thickness less than 3 mm. The finite element method was the first to be developed, and has been used to design several complex repair schemes, such as the repair of fatigue cracks in the lower skin of Mirage aircraft [16], and cracks on the upper surface of the wing pivot fitting of F111C aircraft in service with the Royal Australian AirForce (RAAF), see [17]. Following the development of this approach the work presented in [18] revealed that the stress intensity factor for a patched crack approached a constant value as the crack length increased, thus significantly simplifying the design process. Simple analytical solutions for this asymptotic value were then derived for the case of a patched crack in a thin panel under a remote uniform stress field, [19]. These formulae have subsequently been compared to the values obtained from detailed design charts, see [20], and found to be quite accurate. This approach has largely been superseded by the development of the alternating approach, which enables complex repairs to be analysed in a few minutes on an IBM personal computer, see [21]. In recent years the analytical formulae developed in [19] have also been extended to allow for a disbond in the adhesive directly over the crack [6], see Appendix A. This approach is based on the premise that, for a sufficiently long crack in a structure which is subjected to a remote uniform stress field, the central region of the patch, over the crack, behaves like an overlap joint. From this premise it follows that the stress distribution in this central region should be independent of crack length. (This hypothesis was subsequently confirmed experimentally using thermal emission techniques [22]. Here it was also shown that as the crack grew the rate of change of the energy field with crack length was indeed a constant.) As a result of this analogy the problem of a bonded symmetric lap joint can be used to illustrate the computational tools, and the design methodology, best suited to composite repairs to cracks in thin skins.

Using this analogy the following section will explain the advantage, which is purely computational, of expressing the maximum load carrying capacity P and the "fatigue threshold" load P_f in terms of the quantities W and W_f respectively, rather than the associated stress or strain values.

3.1 Analysis of Symmetric Adhesively Bonded Lap Joints

A schematic representation of the particular symmetric lap joint to be investigated in this section is shown in Figure 10. The adhesive layer has an elastic shear modulus of G_a=750 MPa as determined in section 2.1. The overlap length, l, of the joint is 100 mm. In this analysis the adhesive layer in the double lap joint was kept constant at a realistic value of 0.2mm whilst the adherend thickness, t, was 3.2 mm. The post-yield slope (i.e. the plastic shear modulus) of the adhesive and the yield stress of the adhesive were allowed to vary.

It is known that the maximum stress occurs in the region of the corners 'A' and 'B' of the double lap joint. In the work of Hart-Smith [9], the maximum shear stresses, as derived using an elastic analysis, at these corners was expressed as,

$$\tau = \lambda_e \tau_{av} l/2 \tag{7}$$

where $\tau_{av}l = P/2$, P is the applied load, τ_{av} is the average shear stress and $\lambda_e^2 = 2G_e/Ett_a$. The elastic strain energy at A is thus given by $W_e = \lambda_e^2 \tau_{av}^2 l^2/(8G_e)$, where G_e is the elastic shear modulus of the adhesive.

For large overlap lengths, the shear strains at these corners obtained using an elastic-plastic analysis (Figure 11 shows a schematic representation of the shear stress-strain curve) was also expressed, see [9], as,

$$(\tau_{av}\lambda_e l)/(2\tau_p) = \sqrt{1+2\gamma_p/\gamma_e+(G_p\gamma_p^2)/(G_e\gamma_e^2)} \tag{8}$$

where $\lambda_e^2 = 2G_e/Ett_a$, γ_e and γ_p are the elastic and plastic shear strain at A respectively, τ_p is the yield stress and G_e, G_p are the pre- and post-yield slope of adhesive respectively (see Figure 11). For most aerospace adhesives, G_e is very much larger than G_p. From this result, Hart-Smith [9] subsequently expressed the load carrying capacity of the double lap joint as,

$$P = 2\tau_{av}l = 4\sqrt{Et}\sqrt{((t_a\tau_p\gamma_e)/2)(1+2\gamma_p/\gamma_e+(G_p\gamma_p^2)/(G_e\gamma_e^2))} \tag{9}$$

Defining $\tau_p = G_e\gamma_e$, eqn (9) can be written in terms of the area under the stress-strain curve, viz:

$$P = 4\sqrt{Et}\sqrt{t_a(0.5(G_p\gamma_p^2+G_e\gamma_e^2)+G_e\gamma_e\gamma_p)} = 4\sqrt{Ett_aW_p} \tag{10}$$

where $W_p = 0.5(G_e\gamma_e^2 + G_p\gamma_p^2) + G_e\gamma_e\gamma_p$ is the total area under the shear stress-strain curve. Thus the load carrying capacity of the joint was directly related to the maximum strain energy density of the adhesive.

It will now be shown that the W_p can be estimated from a purely elastic analysis of the joint. The "plastic" shear modulus of the adhesive, G_p, of FM73 and FM300 has been determined experimentally to be very small. For sufficiently long overlap

lengths, the expression for the plastic shear strain (see equation (34) of [9]), can be reduced to,

$$\gamma_p = \lambda_e \gamma_e l \tag{11}$$

With this simplification, the area under the elastic-plastic curve can now be expressed as,

$$W_p = (\lambda_e l)^2(\tau_{av}^2(1+1/(2\lambda_e l))/8G_e + (\tau_p^2 G_p)/(2G_e^2)). \tag{12}$$

Since G_p is small, the contribution of the last term to W_p is small. Therefore, W_p can be approximated by,

$$W_p = (\tau_{av}\lambda_e l)^2/(8G_e) = W_e \tag{13}$$

This expression is the area under the stress-strain curve obtained from a purely elastic analysis. It is important to note that W_e is independent of the elastic modulus of the adhesive. Thus the strain energy as calculated via an elastic-plastic analysis should be independent of the elastic modulus, yield stress and, to a large extent, of the post-yield curve of the adhesive. To confirm this analogy, (i.e. $W_e = W_p$), the preceding approximation was investigated using a finite element analysis of the symmetric lap joint previously described. Table 2 shows the strain energy at the corner 'A' of the joint calculated using the elastic solution and that with an elastic/plastic solution. This corner is chosen as it is the location of the highest stresses.

In calculating the strain energy various stress-strain curves for the adhesive were used with varying values for the yield stress and the post-yield slope. The number of elements, N, used across the adhesive layer was also varied. The strain energy was evaluated for a strain up to a relatively large value (viz: near unity shear strain). The errors between the strain energy as calculated using either a fully elastic solution or an elastic-plastic solution are in the region of 10% (Table 2). From eqn (10) this would correspond to a 5% error in calculating the load carrying capacity of the joint. From Table 2, we also see that for a low post-yield slope, the error is lower than that associated with a high post-yield slope. This is because of the approximation used in eqn (13) where it was assumed that the last term of eqn (12) is small. The error is also observed to increase with an increase in the yield stress. This error is attributed to an increase in the proportion of the elastic strain energy to the total area under the stress-strain curve. However, for realistic values of the yield stresses and the post yield slope this error is only a few percent.

It is also evident from Table 3 that the strain energy thus calculated is relatively independent of the number of elements used across the adhesive layer. Since the strain energy is obtained via numerical integration, it appears to be less susceptible to numerical instability. It is also relatively insensitive to the yield stress and the post-yield slope of the adhesive. As such it is thus an excellent design variable and it is for this reason that W_f is used when calculating the "fatigue threshold" load P_f.

TABLE 2: TABULATED VALUES OF STRAIN ENERGY

Yield Stress (MPa)	Post-yield Slope (MPa)	N	Work		Difference (%)
			Elastic	Plastic	
68	800	4	20.936	22.029	5
68	400	4	20.936	21.981	4
68	100	4	20.936	20.792	1
68	50	4	20.936	20.444	2
140	50	4	20.936	24.724	15
100	50	4	20.936	22.389	7

TABLE 3: TABULATED VALUES OF THE STRAIN ENERGY CALCULATED WITH DIFFERENT VALUES OF N

Yield Stress (MPa)	Post-yield Slope (MPa)	Plastic Work		Difference (%)
		N=1	N=4	
68	50	21.303	20.444	4.2
68	100	19.013	20.792	8.5
68	400	21.270	21.981	3.2

4. ILLUSTRATIVE EXAMPLES

4.1 Repair to Multi-Site Damage

4.1.1 Repair Design

In a series of previous reports [4,6] the authors have presented the results of an experimental test program into the fatigue performance of fuselage lap joints. Particular attention has been paid to joints containing multi-site damage, and both repaired and unrepaired specimens have been tested. In these investigations the test configuration was optimised so as to produce crack growth rates in good agreement with fleet data, see [23].

Before implementing any repair it is necessary to understand the load transfer mechanisms. This was achieved through the use of thermal emission techniques, see [24]. This reference used a detailed three dimensional finite element analysis of the specimen to confirm these results. The model contained 4296 nodes and had 10680 degrees of freedom with the rivets modelled separately using three dimensional isoparametric elements. The experimental investigation revealed that the stress concentration at the first row of rivets decayed very rapidly and that approximately 45% of the load was transferred at the first row of rivets. This was consistent with the value obtained numerically.

As a result of this work it was determined that the provision of an alternative load path with the load by passing the critical region, as in the F111 repair [17], would be a viable repair option. This concept forms the basis of the externally bonded

composite patch described in [2,6]. In this case the maximum (highest) stresses in the adhesive occur when the cracks emanating from each fastener hole have all linked. To determine the magnitude of these stresses a detailed finite element analysis was performed, using the material properties measured in Section 2. The resultant values of maximum stresses and the peak in the strain energy density are given in Table 4.

TABLE 4: LAP JOINT SPECIMEN

Max. Energy (MPa)	Max Shear Stress (MPa)
0.33	4.2

It is thus apparent that, for the proposed repair design, the adhesive stresses are beneath their "threshold" value. This infers that damage should not initiate and that if the adhesive bond was to contain a disbond then this disbond should not grow. To confirm this prediction a series of fatigue tests were performed on repaired specimens containing both in-built disbonds and impact damage.

4.1.2 Experimental Results

The lap joint specimens consisted of two 1.016 mm thick 2024-T3 aluminium sheets fastened with three rows of 3.97 mm diameter BACR15CE-5 100^{o} shear head counter sink rivets. Specimen dimensions are shown in Figure 12. To reproduce crack growth rates in agreement with fleet measurements [23], the specimens were assembled in pairs by bonding back to back on a 12.5 mm thick honeycomb core. Multiple cracks in the upper row of rivets were initiated and grown under a tensile fatigue loading. The specimens were then repaired using a 203 mm long by 203 mm wide unidirectional boron/epoxy doubler. Details of specimen manufacture, crack initiation, crack growth rates and further details of the repair can be found in previous reports [4,23].

Six specimens were used to investigate the damage tolerance of the proposed repair scheme. A summary of the specimen histories, prior to damage tolerance testing, is given in Table 5. Specimens A3, A4 and A5 had experienced a large number of fatigue cycles prior to the application of the impact damage.

Specimens A3, A4 and A5 only contained impact damage, see Table 6, whilst specimen A6 contained both impact damage and adhesive disbonds, and specimens A9 and A10 contained adhesive disbonds, see Figures 13-16. For specimens A9 and A10 a deliberate attempt was made to produce a poor quality bond. In this case the low temperature curing adhesive Flexon 241 was used, which has an inferior durability performance, see [1].

4.1.3 Fatigue Test Procedure

Fatigue testing was conducted in a 1 MN Instron servo-hydraulic test machine. The damaged specimens were subjected to a constant amplitude tensile fatigue loading

with P_{max} = 40 kN and P_{min} = 2 kN, at a frequency of 2.5 Hz. This loading represents the hoop stress in the fuselage skin due to pressurization, refer [4]. Testing was continued until failure of the specimen occurred, or a sufficient number of cycles had been accumulated to demonstrate the effectiveness of the repair.

The condition of the impacted specimens was monitored throughout the test using the shadow moire technique. A detailed description of this technique and its application to monitoring damage growth is given in [25].

TABLE 5. SPECIMEN HISTORY

Specimen No.	Fatigue Cycles			
	Precracking	Unrepaired	Repaired	Enviromental
A3	178,400	-	2,155,550	1,062,400
A4	178,400	-	2,155,550	1,062,400
A5	5,000	41,400	1,300,070	-
A6	5,000	25,000	-	-
A9	19,210	110,030	-	-
A10	19,210	105,700	-	-

TABLE 6. IMPACT RESULTS

Specimen No.	Impactor Mass (g)	Impact Site	Impact Energy (J)
A3	200	1	1.6
		2	1.7
		3	1.2
A4	200	1	1.7
		2	2.0
		3[a]	-
		4	1.4
A5	400	1	4.0
		2	3.7
A6	400	1	4.0
		2	4.2

a - impact energy not recorded

4.1.4 Fatigue Test Results

The number of fatigue cycles applied to each of the specimens is shown in Table 7. None of the repairs showed any significant sign of failure or degradation during the tests. This contrasts with an average life of 75,000 cycles for the unrepaired specimens, refer [4].

More than 1,000,000 cycles were applied to specimens A9 and A10 without failure of the repairs. It should be noted for these specimens that, prior to repair, the cracks at the first row of rivets had propagated across the entire width of the specimen (i.e. the specimen had failed). Despite the deliberate poor quality of these repairs, and in

particular the large disbond area in specimen A10, the composite doubler was able to carry the load without further degradation.

Specimen A6 withstood more than 1,400,000 cycles without failure or apparent disbond growth.

After impacting, specimens A3 and A4 were subjected to in excess of 450,000 cycles. These failed by fatigue crack growth in the aluminium sheet outside the repair. It should be noted that these specimens had accumulated a total of more than 3,000,000 load cycles during previous testing. There was no sign of degradation or failure of the repair. An eddy current inspection of the specimens was conducted to determine the extent of crack growth since impacting. It was found that no further crack growth had occurred during this test program. Specimens A5 and A6 withstood 180,000 cycles after impacting, again with no apparent degradation or failure.

4.1.5 Tension Tests

On completion of these fatigue tests four specimens, namely A3/A4 and A9/A10, were loaded to failure in tension in order to determine the strength of the damaged repair. For the purpose of comparison an undamaged and unrepaired, i.e. "as new", lap joint specimen pair was also tested. In each case, the load was applied at a rate of 37.5 kN/min. The specimen pair A3/A4, which had previously failed outside of the patched region, was repaired to enable the tensile test to be conducted.

The tension test results are shown in Table 8. The repaired specimens exceeded the strength of the "as new" lap joint specimen. Specimens A3/A4 failed in the aluminium sheet outside the repair area, while specimens A9/A10 failed by debonding and tearing of the composite doublers. The significantly lower strength of specimens A9/A10 was expected due to the poor quality of the bond. Despite this, the strength of these fatigued specimens still exceeded the strength of the standard, "as new" lap joint.

4.1.6 Concluding Remarks

This test program has demonstrated that the presence of adhesive disbonds, and damage due to low velocity impacts, does not degrade the boron/epoxy repairs and that the multi-site damage beneath the repair does not grow. This was shown by demonstrating that the fatigue life of the repaired specimens, containing damage, far exceeds that of an unrepaired lap joint specimen. Inspection of the specimens during and after testing revealed no damage growth. In addition, it was shown that the static strength of the damaged repairs exceeds that of an uncracked lap joint.

TABLE 7. FATIGUE TEST RESULTS

Specimen No.	Type of Damage	Fatigue Cycles
A3[a]	impact	454,670
A4[a]	impact	454,670
A5	impact	180,000
A6	disbond	1,316,470
	impact	180,000
A9	disbond	1,000,000
A10	disbond	1,004,330

a - specimen failed by fatigue in aluminium sheet outside repair area

TABLE 8. TENSILE TEST RESULTS

Specimen	Total Fatigue Cycles	Static Failure Load (kN)
Undamaged Lap Joint	0	116
A3/A4	3,672,570	161
A9/A10	1,110,030	121

4.2 Repair to Edge Notch Specimens

4.2.1 Repair Configuration

The test specimen consisted of a 6 mm edge crack in a 3.66 mm (5/32") thick 2024-T3 aluminium alloy sheet, with dimensions 145 mm by 480 mm, repaired with a twelve ply unidirectional boron-epoxy patch. The patch contained in-built disbonds, which were simulated using teflon inserts. The teflon inserts measured 6 mm by 4 mm. Three disbond configurations were evaluated; viz:

1) Four specimens with a teflon insert directly over the crack.

2) Four specimens with a teflon insert at the edge of the patch.

3) Two specimens with teflon inserts directly over the crack and at the edge of the patch.

The specimens were fatigued, under load control, in a servo-hydraulic Instron test machine under constant amplitude loading, with R=0.05 and a remote stress amplitude, in the aluminium, of 137.9 MPa. These tests were performed in a hot, 65°C, wet aggressive environment. Prior to testing the patched specimens were pre-conditioned to a moisture content of 1 %, by weight, in a 5 % salt solution. After

achieving this moisture content the specimens were sealed to prevent moisture from escaping. All specimens were tested immediately after pre-conditioning. This process mirrors that described, in more detail, in [23].

4.2.2 Analysis

As in the previous example a detailed three dimensional finite element analysis of the repaired specimen was undertaken. Due to symmetry only one half of the structure was modelled using twenty noded isoparametric brick elements and fifteen noded isoparametric wedge elements, see Figure 17. The resultant values of maximum shear stresses and the peak in the strain energy density are given in Table 9.

TABLE 9: EDGE NOTCH SPECIMEN

Max. Energy (MPa)	Max Shear Stress (MPa)
0.222	3.3

It is thus apparent that for the proposed repair design the adhesive stresses are below their "threshold" value. This again infers that damage should not initiate and that, if the adhesive bond was to contain a disbond then this disbond would not grow. To confirm this prediction a series of fatigue tests were performed in a hot, 65^{o}C, wet aggressive environment, on repaired specimens containing in-built disbonds (delaminations).

4.2.3 Test Results

After 50,000 cycles none of the specimens showed any sign of damage growth. During this period the maximum extent of crack growth observed in any of the specimens was less than 1.75 mm. As a result, since the fatigue life of the unrepaired specimens was less than 9,000 cycles, see [1], it was decided to stop testing of the repaired specimens after 50,000 cycles.

The lack of damage growth in any of these specimens supports the results of the PABST program as well as the design methodology outlined in Section 2.

5. CONCLUSION

This report has confirmed the design approach developed as part of the PABST program, [8], viz: that adhesively bonded repairs to thin skins are inherently damage tolerant, provided that the adhesive stresses and strains are beneath their threshold values. These threshold values have been presented for the thin film adhesive FM73, which is widely used in repair applications. The stress/strain response of this adhesive, at various strain rates, together with the associated value of W_f is also presented, as is an analytical representation for this, rate dependent, response.

6. REFERENCES

1. A. A. Baker and R. Jones, Bonded Repair of Aircraft Structures, Martinus Nijhoff, The Netherlands, 1988.

2. R. A. Bartholomeus, J. J. Paul and J. D. Roberts, Application of bonded composite Repair technology to Civilian Aircraft- 747 Demonstrator Program, Proceedings International Conference on Aircraft Damage Assessment and Repair, ed by R. Jones and N. J. Miller,Published by The Institution of Engineers Australia, ISBN (BOOK) 85825 537 5, July 1991.

3. J. L. Taylor, The Practicalities of Ensuring the Continued Structural Integrity of Aging Aircraft in an Airline Environment, Proceedings International Conference on Aircraft Damage Assessment and Repair, ed by R. Jones and N. J. Miller, Published by The Institution of Engineers Australia, ISBN (BOOK) 85825 537 5, July 1991.

4. R. Jones, N. Bridgford, L. Molent and G. Wallace, Bonded repair of multi-site damage, pp 199-213, Structural Integrity of Aging Airplanes, edited by S. N. Atluri, S. G. Sampath and P. Tong, Springer Verlag, Berlin/Hieldelberg, 1991.

5. C. Torkington, The regulatory aspects of the repair of civil aircraft metal structures, Proceedings International Conference on Aircraft Damage Assessment and Repair, ed by R. Jones and N. J. Miller, Published by The Institution of Engineers Australia, ISBN (BOOK) 85825 537 5, July 1991.

6. R.Jones, Recent developments in advanced repair technology, Proc. Int. Conf. on Aircraft Damage Assessment and Repair, Melbourne, August 1991, Published by Institution of Engineers Australia, ISBN (BOOK) 85825 5375, July 1991.

7. E. W. Thrall, Primary adhesively bonded structure technology (PABST): Design handbook for adhesive bonding, USAF Technical Report, AFFDL-TR-79-3119, 1979.

8. L. J. Hart-Smith, Design and analysis of bonded repairs for metal aircraft structures, Chapter 3, Bonded Repair of Aircraft Structures, edited by A. A. Baker and R. Jones, Martinus Nijhoff, The Netherlands, 1988.

9. L. J. Hart-Smith, Adhesively bonded double lap joints, NASA Langley Research Center Report NASA CR-112235, January 1973.

10. ASTM D 1002, Standard test method for strength properties of adhesives in shear by tension loading (Metal to Metal), ASTM Standards Vol.15.06 Sec. 15 ASTM, Philadelphia, pp 45, 1990.

11. J. Sweeney and I. M. Ward, A unified model of stress relaxation and creep applied to oriented polyethylene, J. Materials Science, 25, pp697-705, 1990.

12. I. M. Ward, Mechanical Properties of Solid Polymers, Wiley Interscience Publication, New York, 1990.

13. M. Kitagawa, T. Mori and T. Matsutani, Rate dependent non-linear constitutive equation of polypropylene, J. Polymer Science, 27,1, pp 85-95, 1990.

14. V. G. Ramaswamy, A constitutive model for the inelastic multi-axial cyclic response of the nickel based super alloy, Rene 80, NASA CR 3998, July 1986.

15. E. P. Cernocky, Comparison of the unloading and reversed loading behaviour of three visco-plastic constitutive theories, 17, 4, pp 255-266, J. Materials Science, 1982.

16. A. A. Baker, R. J. Callinan, M. J. Davis, R. Jones and J. G. Williams, Repair of Mirage iii aircraft using BFRP crack patching technology, Theoretical and Applied Fracture Mechanics, 2, 1, 1-16, 1984.

17. L. Molent, R. J. Callinan and R. Jones,Design of an all boron epoxy doubler for the F111C wing pivot fitting: Structural Aspects, Composite Structures 11, 1, 57-83, 1989.

18. S. N. Atluri and M Kathiresan, Stress analysis of typical flaws in aerospace structural components using 3-D hybrid displacement finite element method, 19the AIAA/ASME Structures, Structural Dynamics and Materials Conference, pp 340-350, 1978.

19. L. R. F. Rose, A cracked plate repaired by bonded reinforcements, Int. J. Fracture, 18, 135-144, 1982.

20. R. Jones and R. J. Callinan, A design study in crack patching, Aeronautical Research Laboratory Structures Report 376, 1979.

21. S. N. Atluri and P. Tong, Computational schemes for integrity analysis of fuselage panels in aging airplanes, Structural Integrity of Aging Airplanes, edited by S. N. Atluri, S. G. Sampath and P. Tong, Springer Verlag, Berlin/Hieldelberg, 1991.

22. R. Jones, M. Heller, D. Lombardo, S. Dunn, J. Paul and D. Saunders, Thermoelastic Assessment of damage growth in composites, Composite Structures, 12, 291-314, 1990.

23. L. Molent, N. Bridgford, D. Rees and R. Jones, Environmental evaluation of repairs to fuselage lap joints, Composite Structures, 21, no. 2, 121-130, 1992.

24. R. Jones, D. Rees and R. Kaye, Stress analysis of fuselage lap joint, Int. Workshop on Structural Integrity of Aging Airplanes, Atlanta, 31st March to 2nd April 1992, edited by S. N. Atluri, C. Harris, A. Hoggard, W. Jones, N. J. Miller, and S. G. Sampath.

25. K. C. Watters, J. G. Sparrow and R. Jones, Shadow Moire monitoring of damaged graphite epoxy specimens, Structures Technical Memorandum 398, Aeronautical Research Laboratories, DSTO, February 1985.

26. P. Davies, C. Moulin and H. Kaush, " Measurement of G1c and G11c in carbon/Epoxy composite", Comp. Science and Technology, 39, pp193-205, 1990.

27. T. Swift, Repairs to damage tolerant aircraft, Structural Integrity of Aging Airplanes, edited by S. N. Atluri, S. G. Sampath and P. Tong, Springer Verlag, Berlin/Hieldelberg, 1991.

APPENDIX A: Formulae for the Stress Intensity Factor of a Crack Repaired with a Composite Patch.

After patching, the stress intensity factor for a crack in a thin skin, under a remote uniaxial stress σ_0, approaches an asymptotic value K_∞,which is independent of the length of the crack. This value of K_∞ can be approximated by the formulae;

$$K_\infty = \sigma_0\sqrt{\pi\lambda} \tag{A.1}$$

where

$$\pi\lambda = \sqrt{E_p t_p/\beta(1+t_p E_p/E_r t_r)} \tag{A.2}$$

$$\sigma_0 = \sigma E_p t_p/(E_p t_p+E_r t_r) \tag{A.3}$$

and

$$\beta = (t_a/G_a+t_r/3G_r+t_p/3G_p)/(t_a/G_a+3t_r/8G_r+3t_p/8G_p)^2 \tag{A.4}$$

where t_a, t_p and t_r are the thicknesses of the adhesive, plate, and patch respectively, G and E denote the shear and Youngs modulus and the subscripts a, p and r denote their values for the adhesive, plate, and patch respectively.

If the patch has disbonded over the entire length of the crack the resultant energy release rate can be estimated from the formulae

$$G = K_\infty^2/E + \sigma^2 L(t_p/t_r)/(2E_r(1+t_r E_r/E_p t_p)) \tag{A.5}$$

where K_∞ is the value of the stress intensity factor for the case when there is no disbond and the total length of disbond perpendicular to the crack is 2L.

To illustrate the accuracy of these simple formulae we will consider two cases.

Case 1. A centrally located crack, 38 mm long, in a rectangular sheet of aluminium alloy with dimensions 300 mm x 320 mm x 2.29 mm. The crack is patched with a uni-directional boron epoxy laminate with dimensions 160 mm x 160 mm x 0.762 mm. The adhesive is 0.1 mm thick and has a shear modulus of 700 MPa. The moduli of the boron epoxy laminate are taken as

$$E_{11} = 208.3 \text{ GPa}, \quad E_{22} = 24.5 \text{ GPa}, \quad \nu_{12} = 0.1667, \quad G_{12} = 7.24 \text{ GPa}$$

substituting these values into equations (A.1) to (A.4) gives the ratio of the stress intensity factors to be $K_\infty/K_u = 0.16$, where K_u is the unpatched value of the stress intensity factor, which compares favourably with the value of 0.19 given in [20].

Case 2. As above, but with the patch containing a rectangular disbond, over the entire length of the crack, with dimensions 25.4 mm x 38 mm, i.e. L= 12.7 mm.

Substituting these values into equation (A.5) gives the stress intensity factor K, where $G=K^2/E$, to be

$$K = 0.447\ K_u \qquad (A.6)$$

which compares favourably with the value of $0.381K_u$ given in [20]. Here we have used the result of case (1) that without a disbond $K_\infty = 0.19\ K_u$.

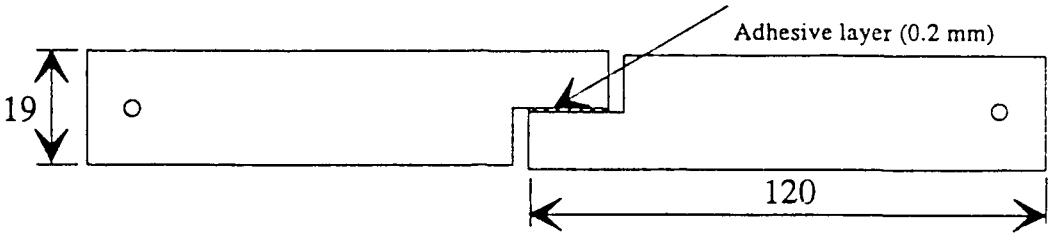

All dimensions in mm

Figure 1: Schematic drawing of the lap shear specimen.

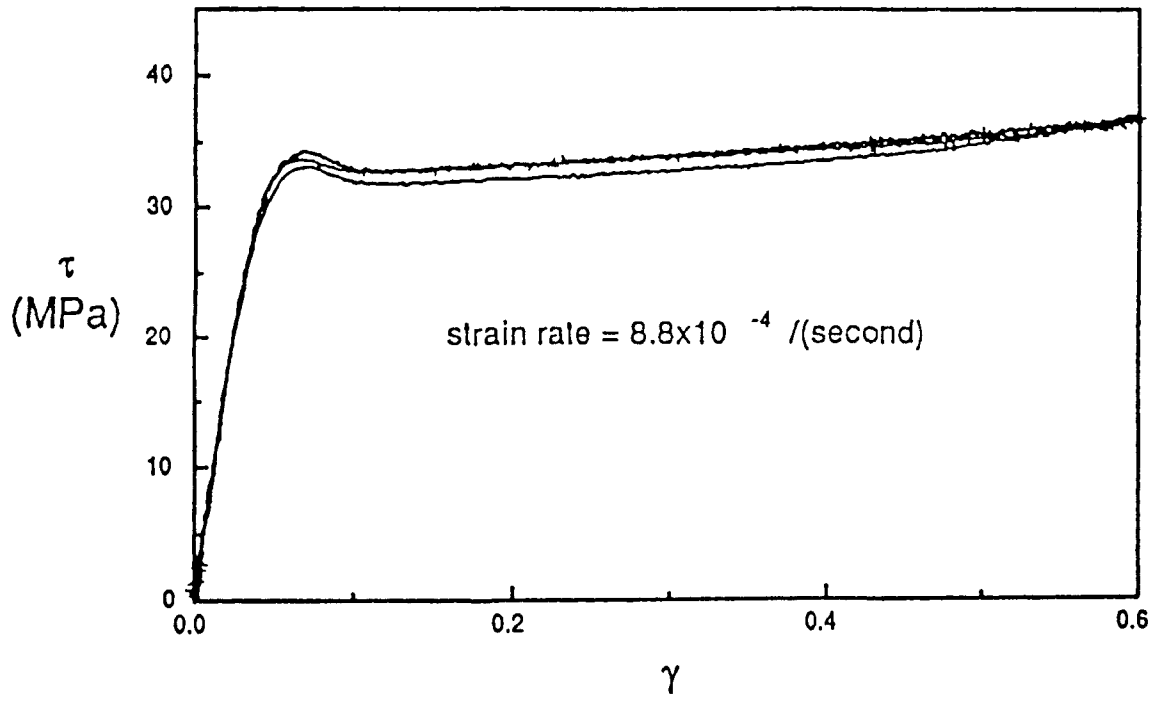

Figure 2: Shear stress vs shear strain (at strain rate 8.78e-4).

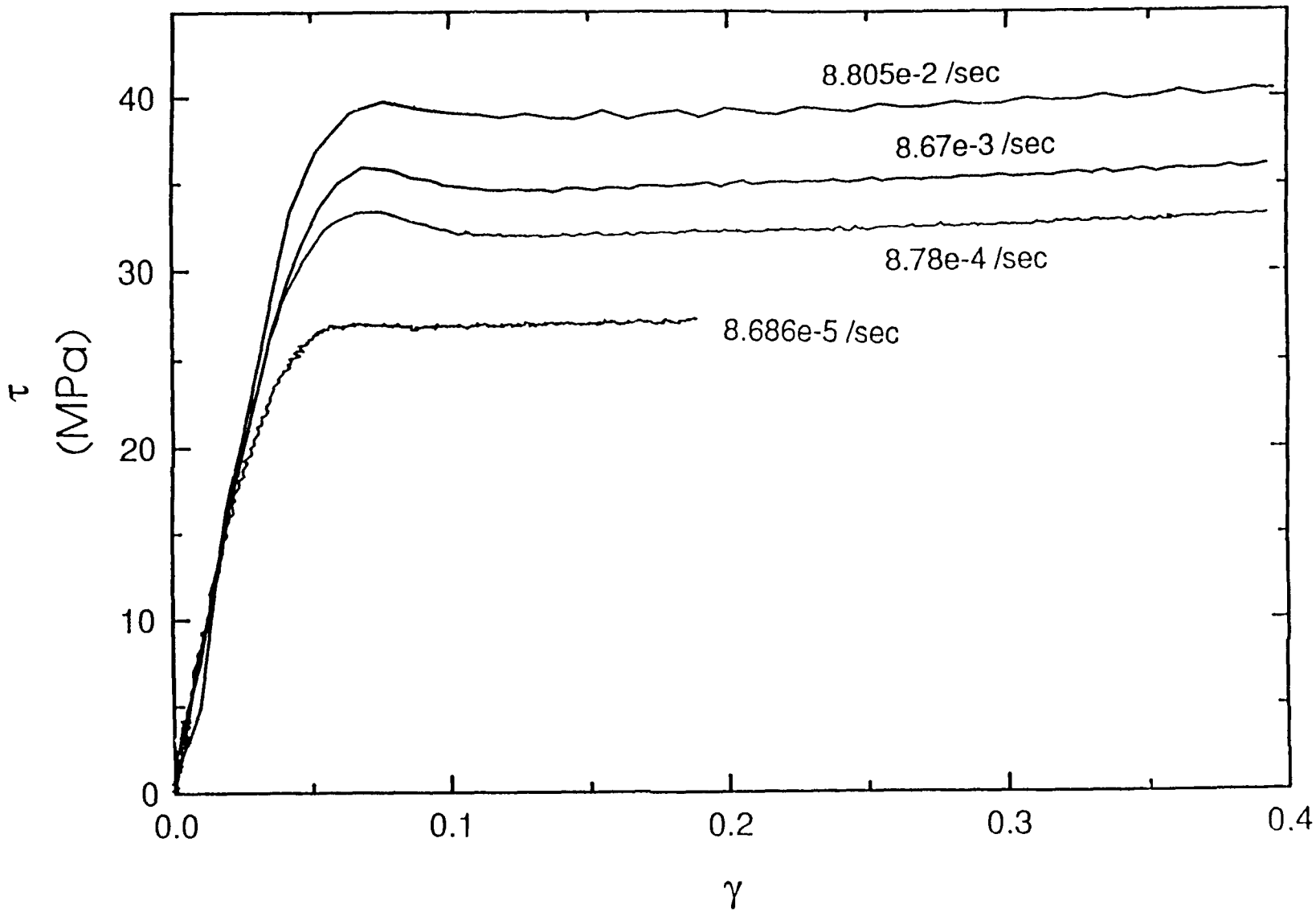

Figure 3: Shear stress vs shear strain at various strain rates.

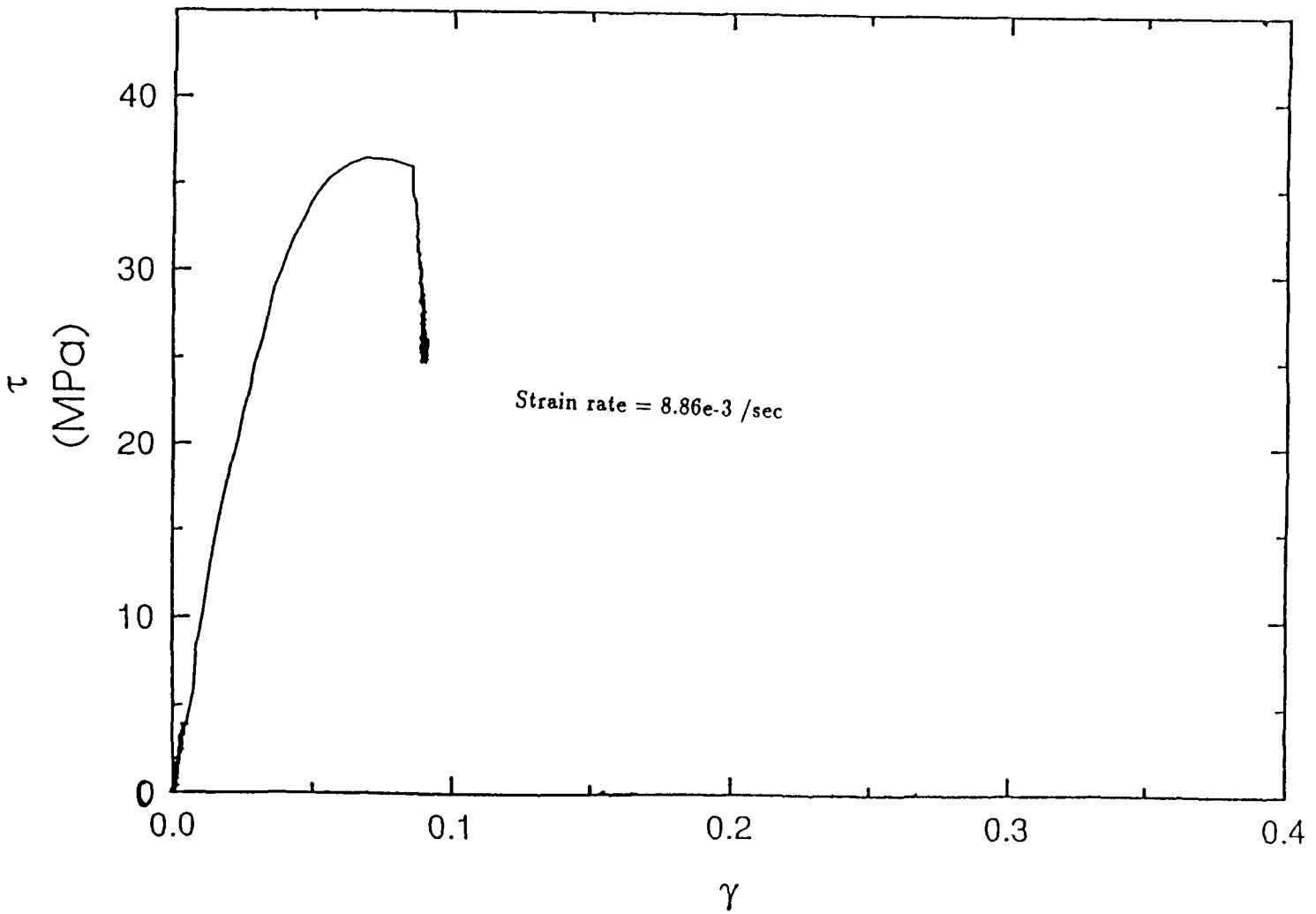

Figure 4: Stress relaxation during a strain hold.

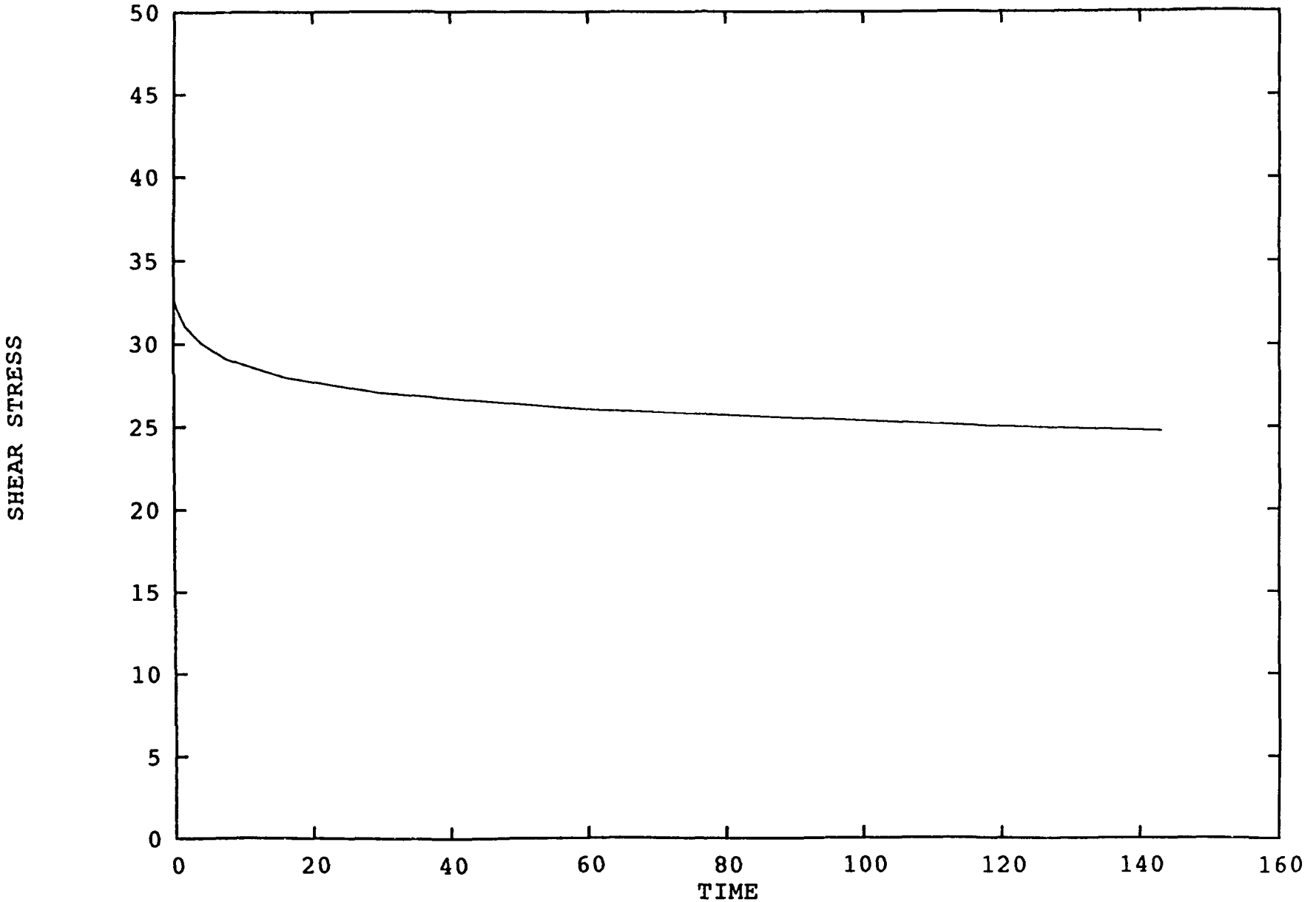

Figure 5: Temporal stress decay during a strain hold.

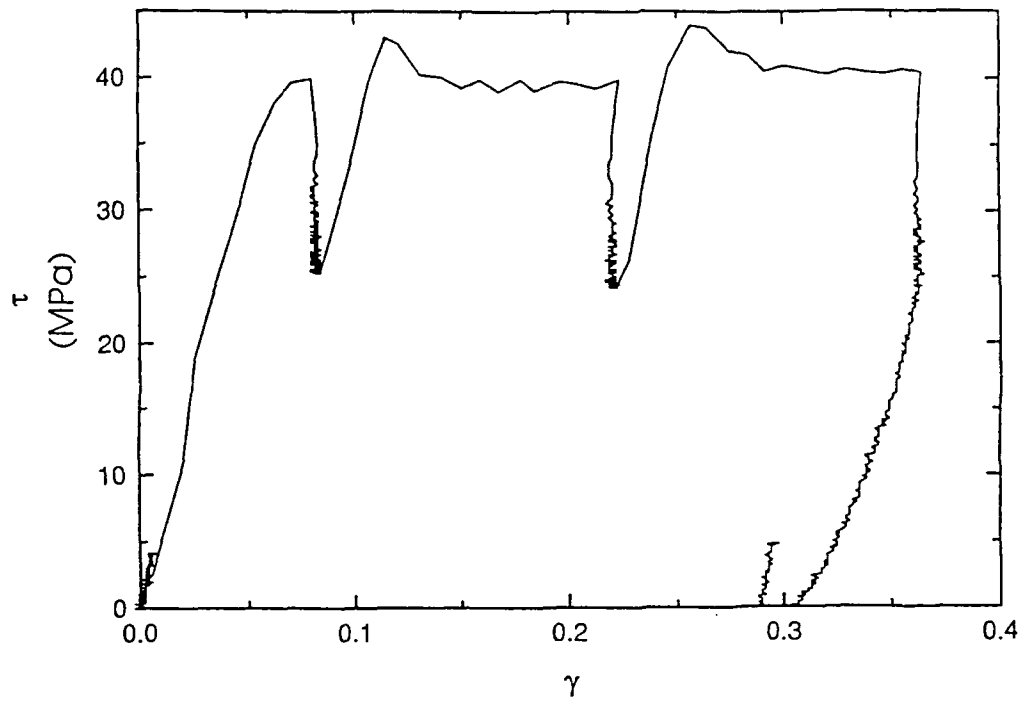

a

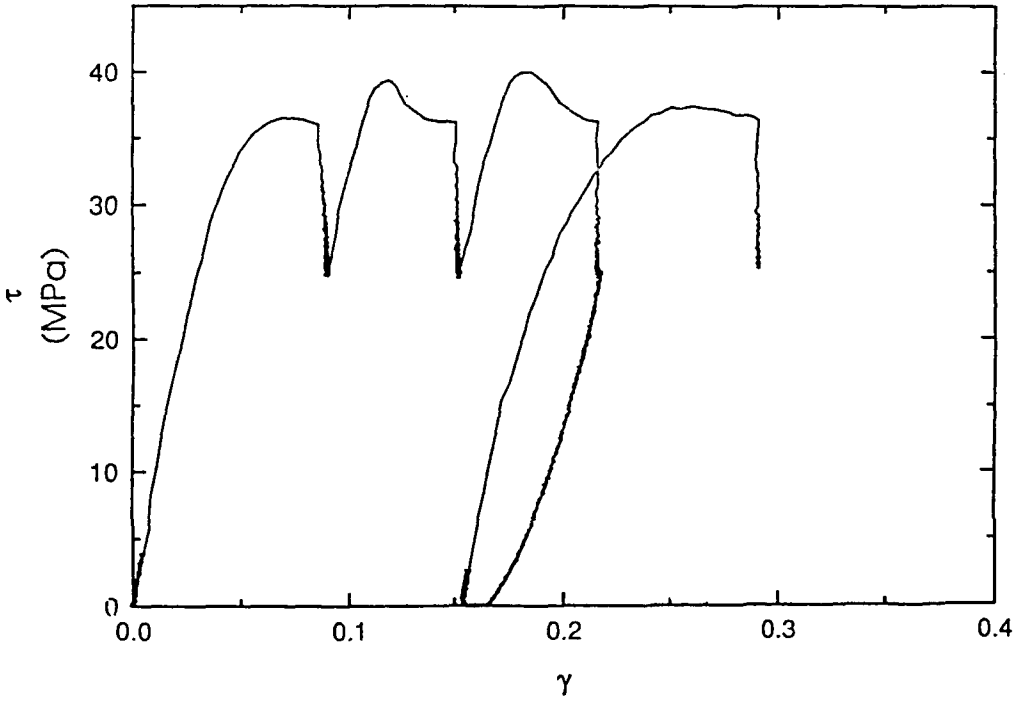

b

Figure 6: Stress relaxation during two strain holds
(a - 8.80e-2 /sec; b - 8.67e-3 /sec).

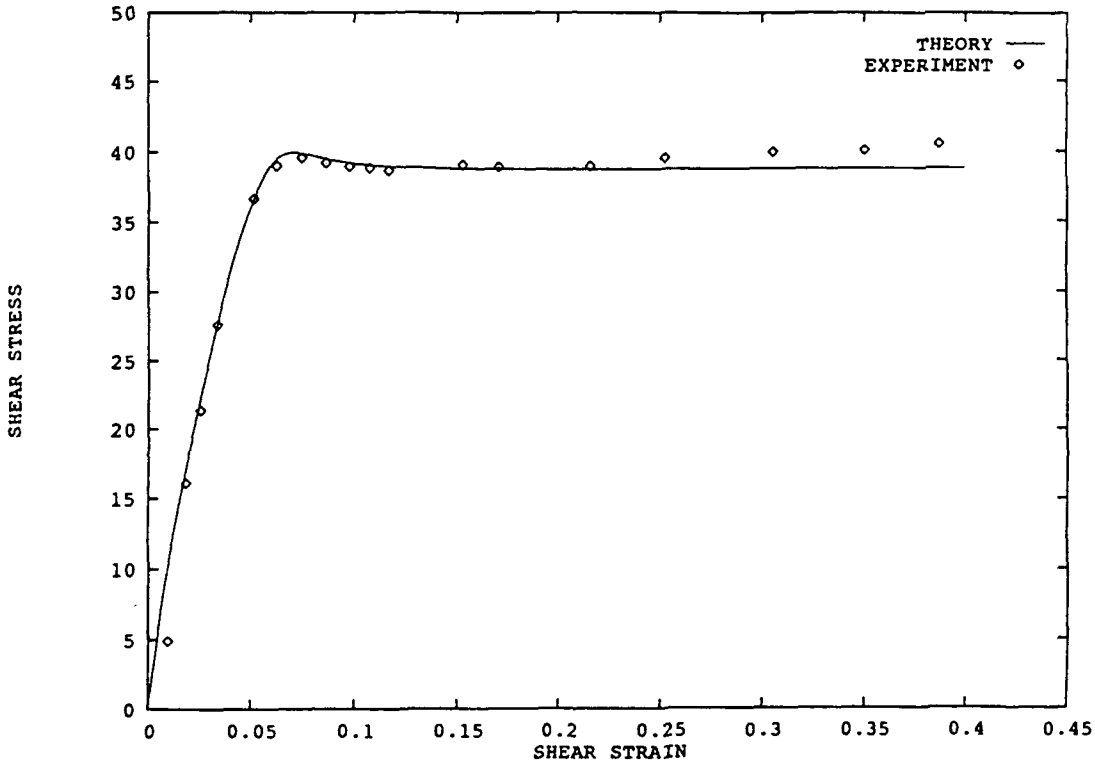

Strain rate = 8.86e-2 /sec

Figure 7: Comparison between experimental and theoretical stress/strain curves.

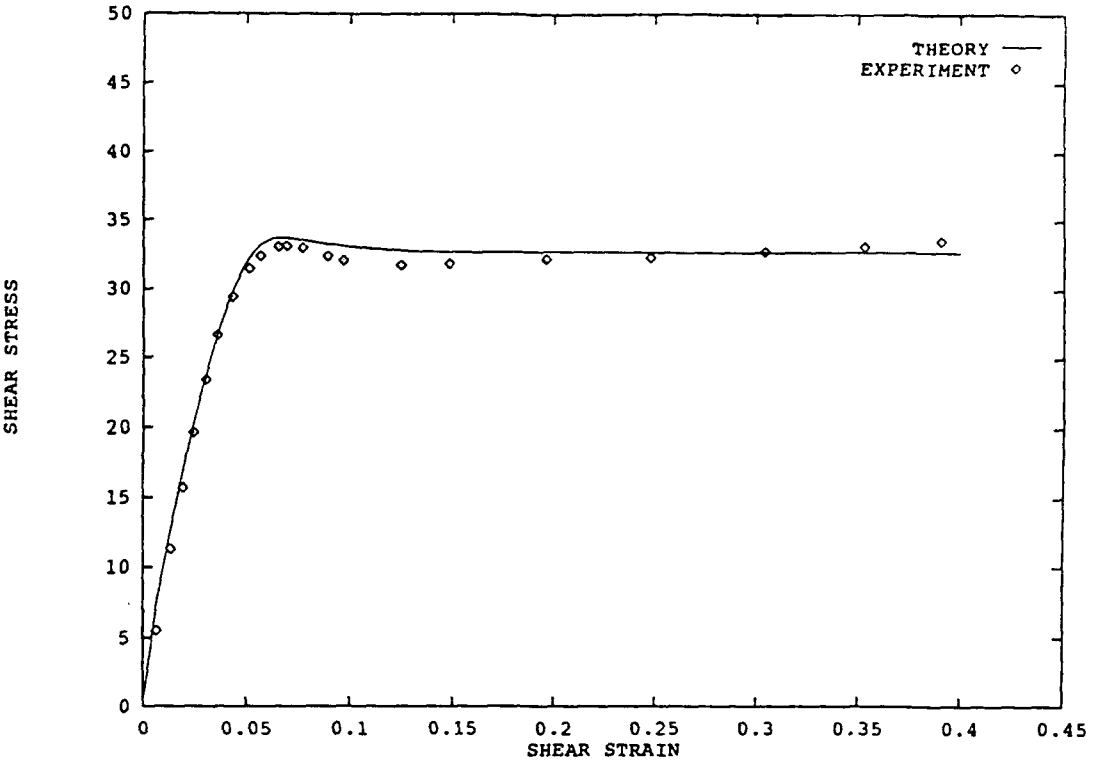

Strain rate = 8.86e-4 /sec

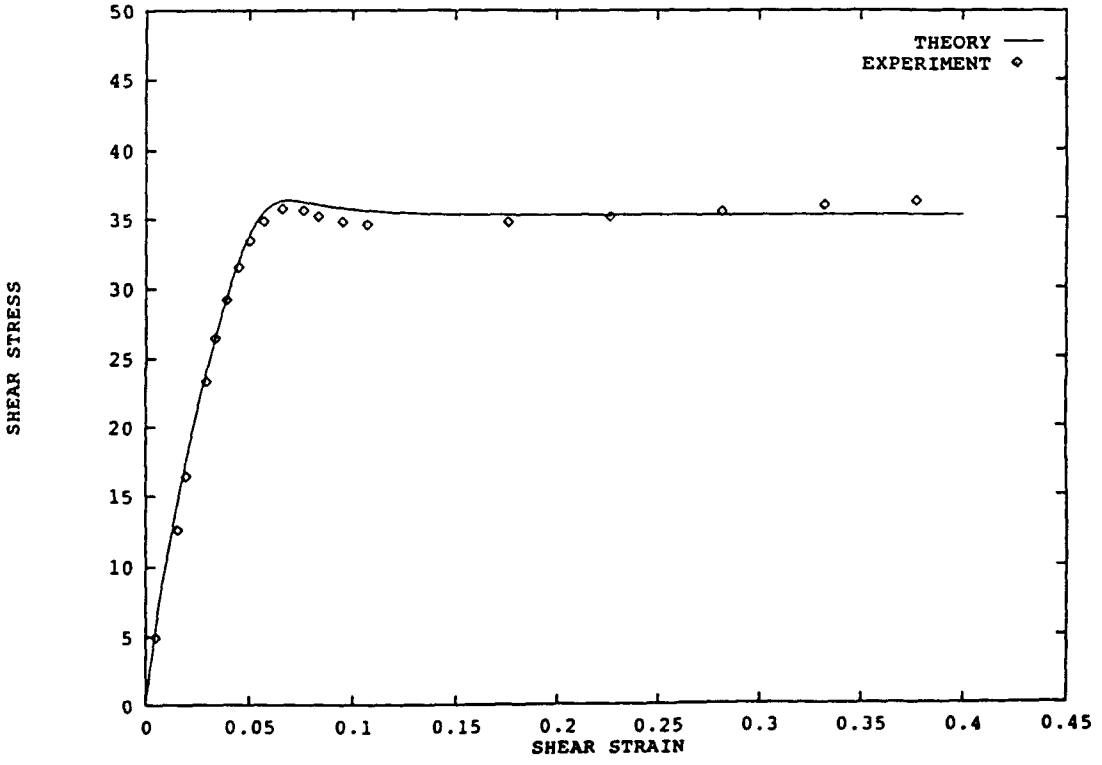

Strain rate = 8.86e-3 /sec

Figure 7

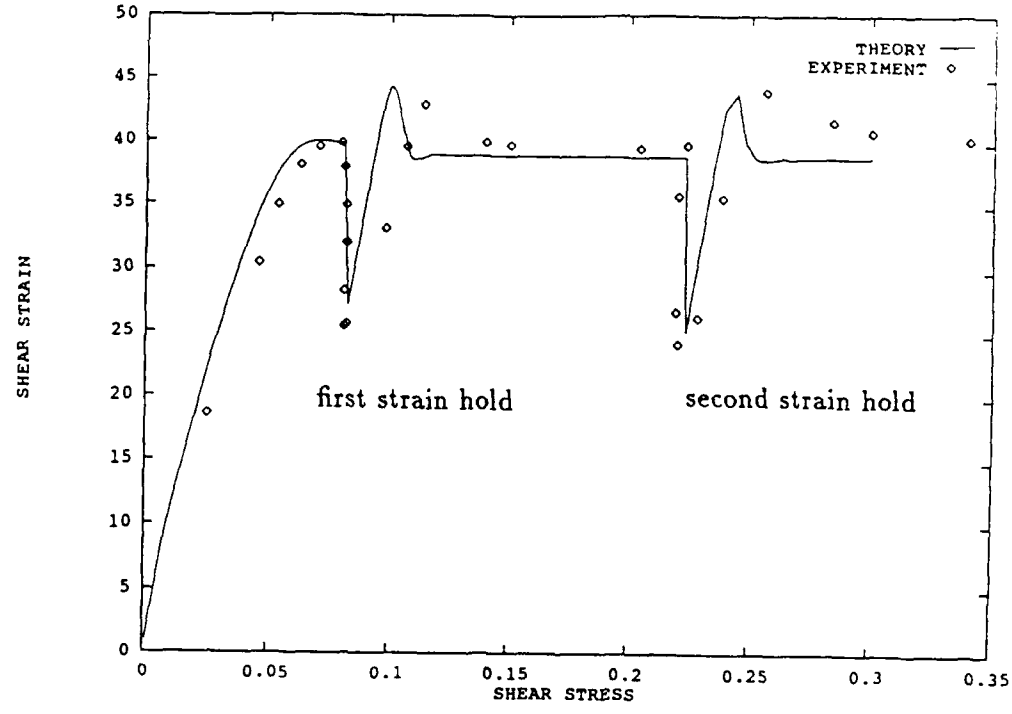

a Strain rate = 8.80e-2 /sec

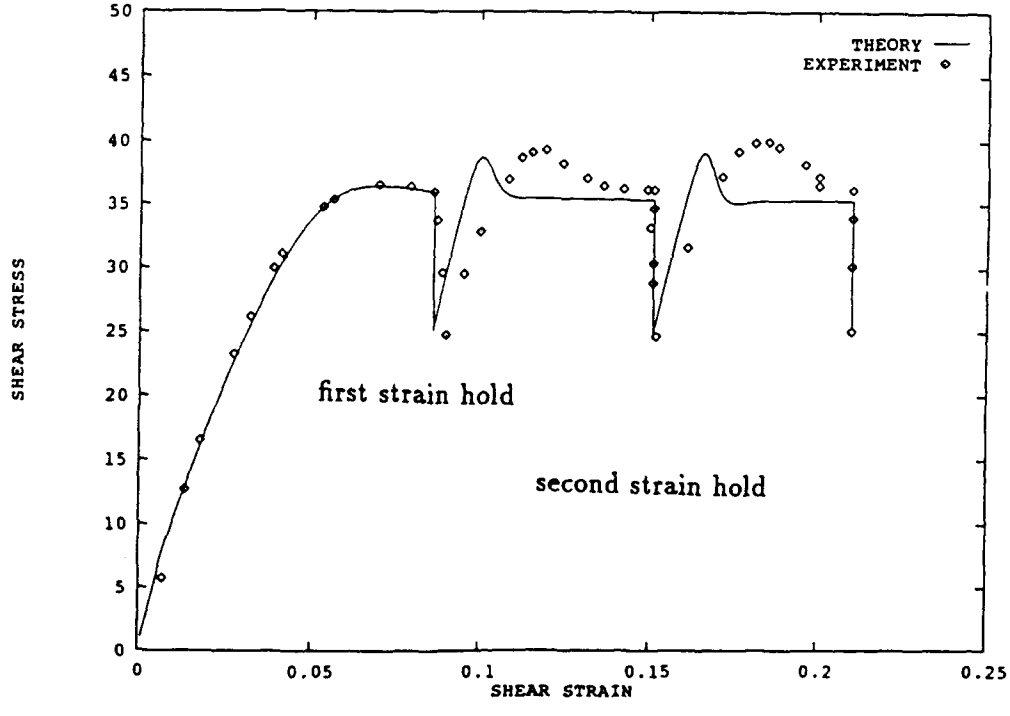

b Strain rate = 8.820e-3/sec

Figure 8: Predicted stress relaxation during strain hold

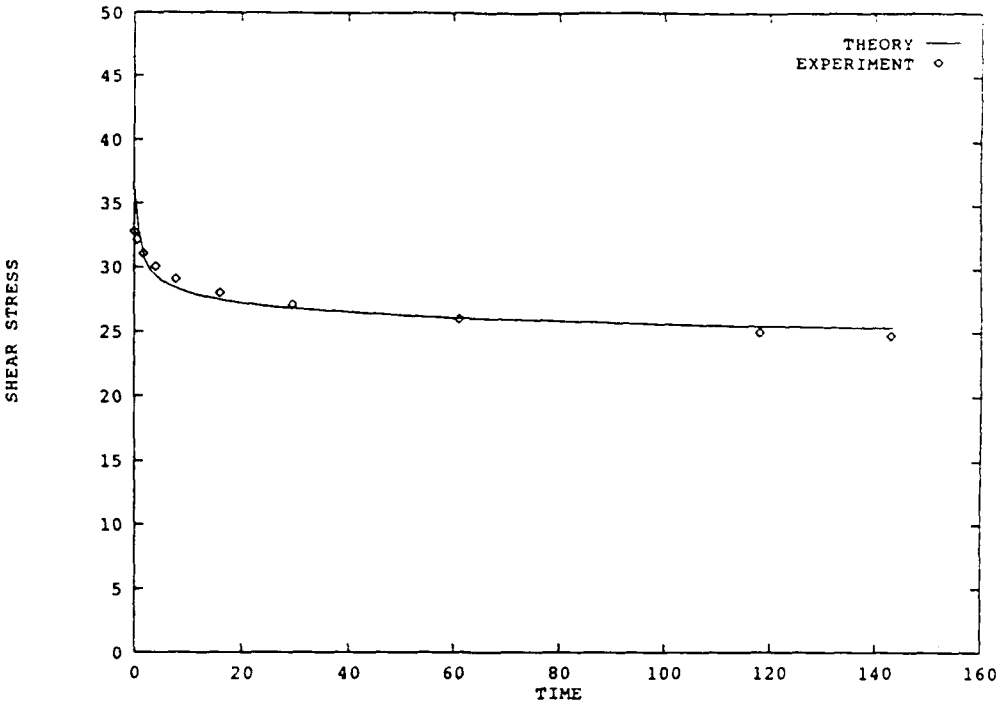

Strain rate = 8.86e-3 /sec; Stress decay during first strain hold.

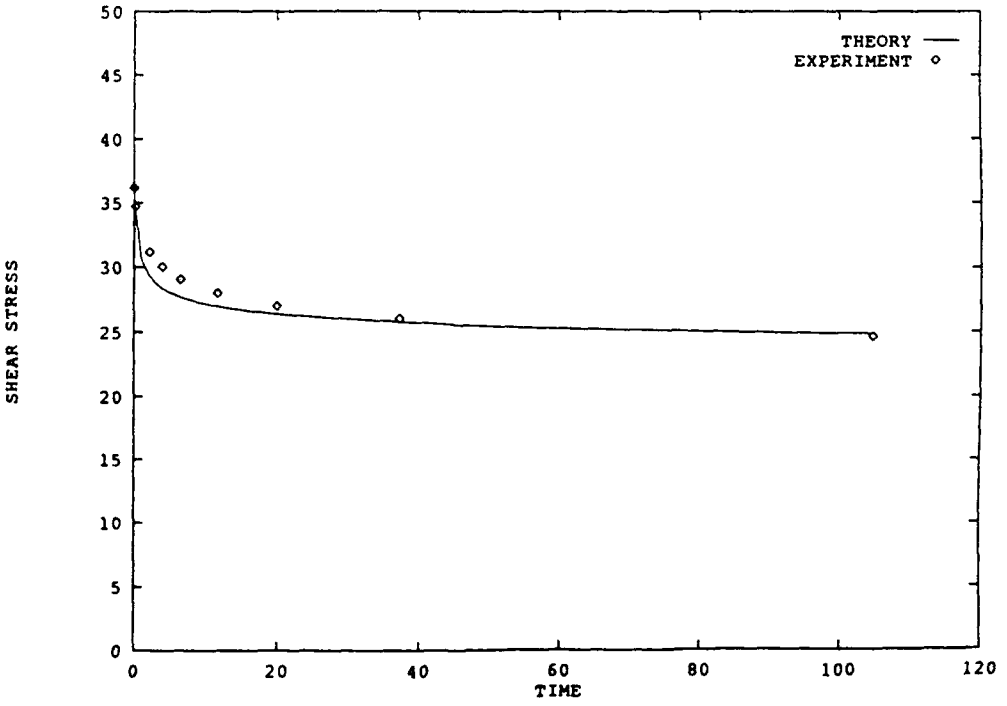

Strain rate = 8.86e-3 /sec; Stress decay during second strain hold.

Figure 9: Predicted temporal stress decay during strain hold.

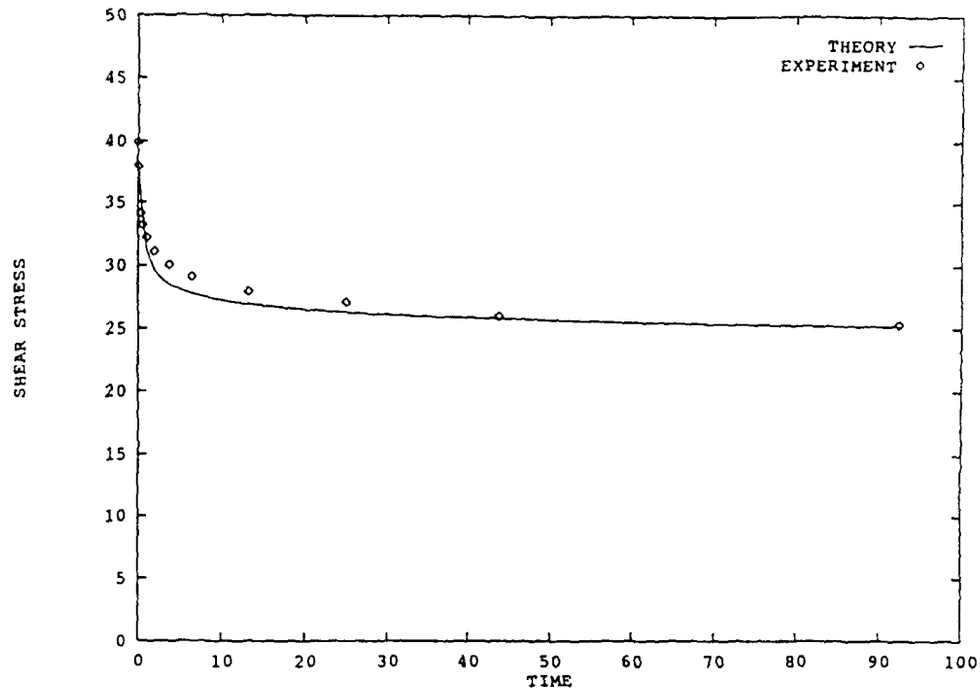

Strain rate = 8.86e- 2 /sec; Stress decay during first strain hold.

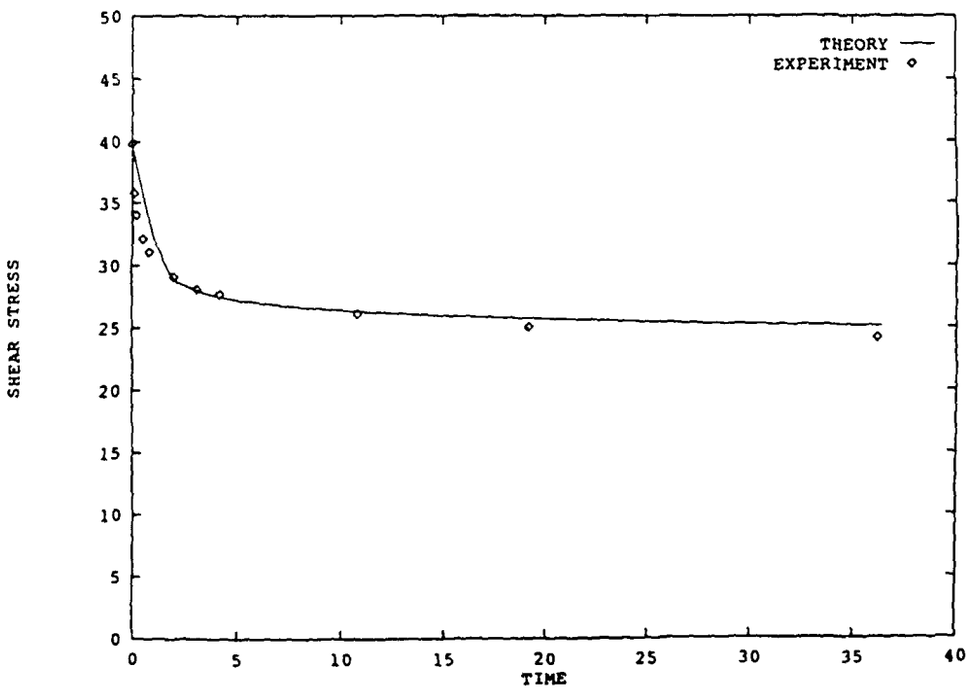

Srain rate = 8.86e-2 /sec; Stress decay during second strain hold.

Figure 9

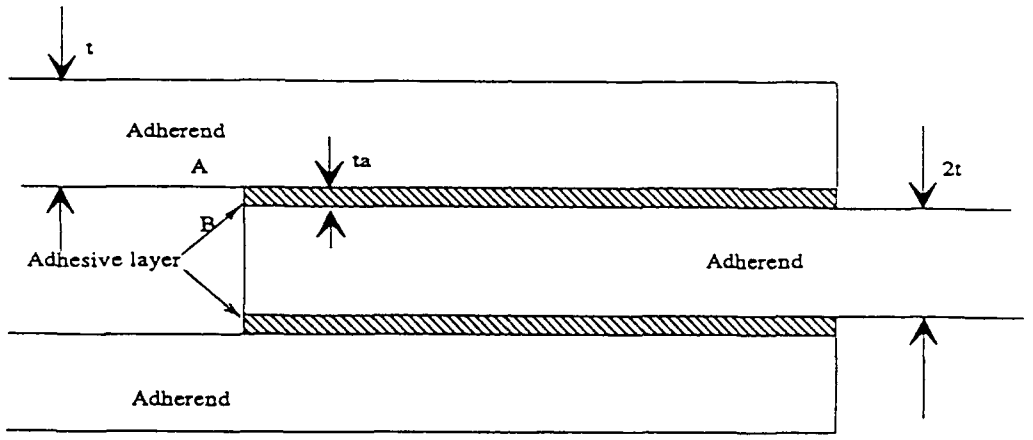

Figure 10: Schematic representation of the double lap joint.

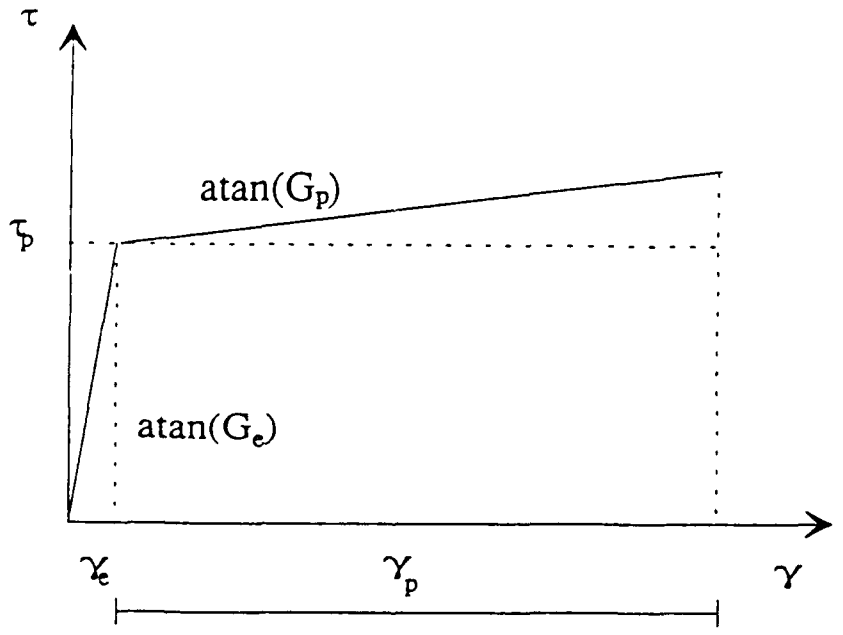

Figure 11: Schematic representation of stress/strain curve.

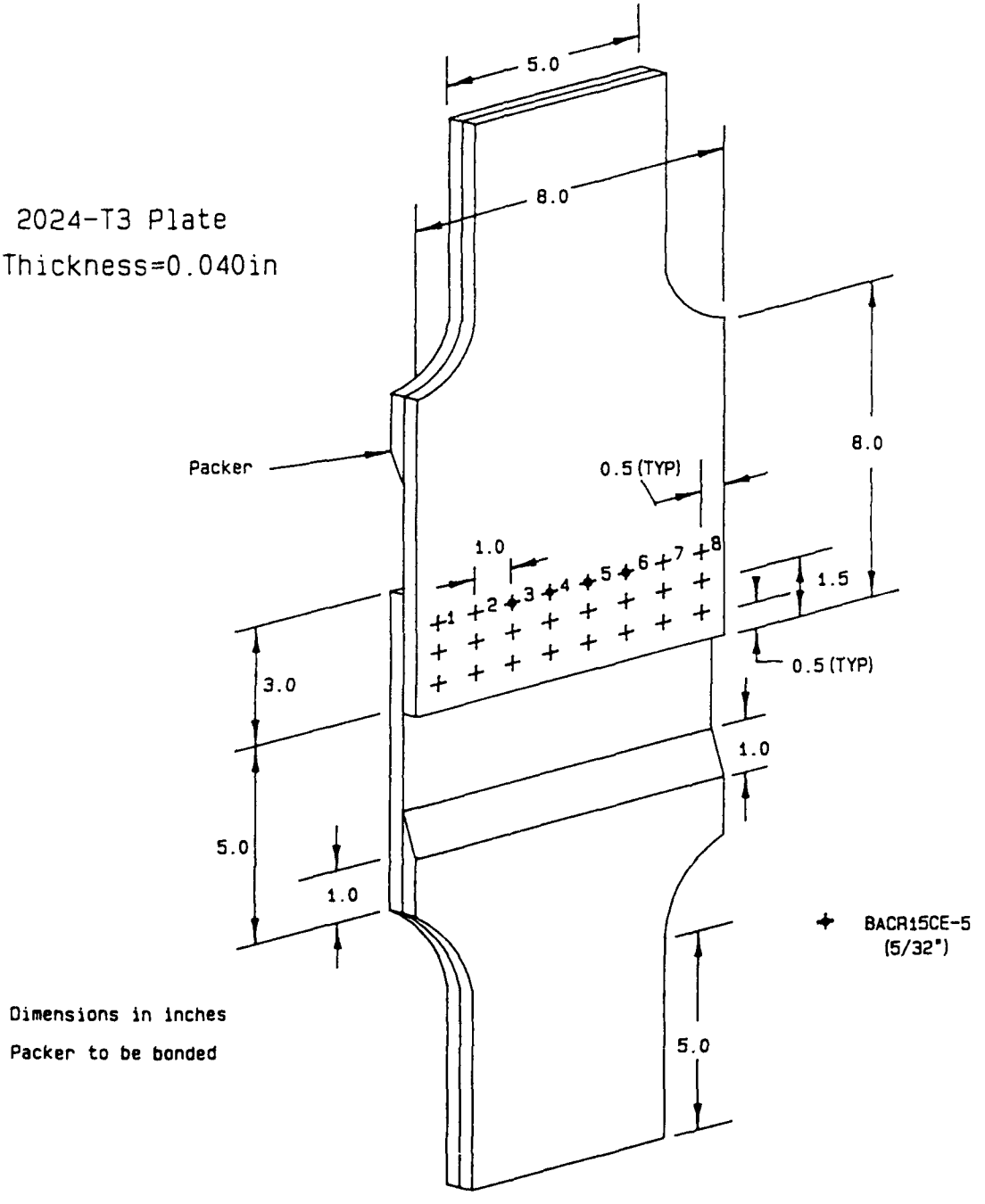

Figure 12: Fuselage lap joint specimen.

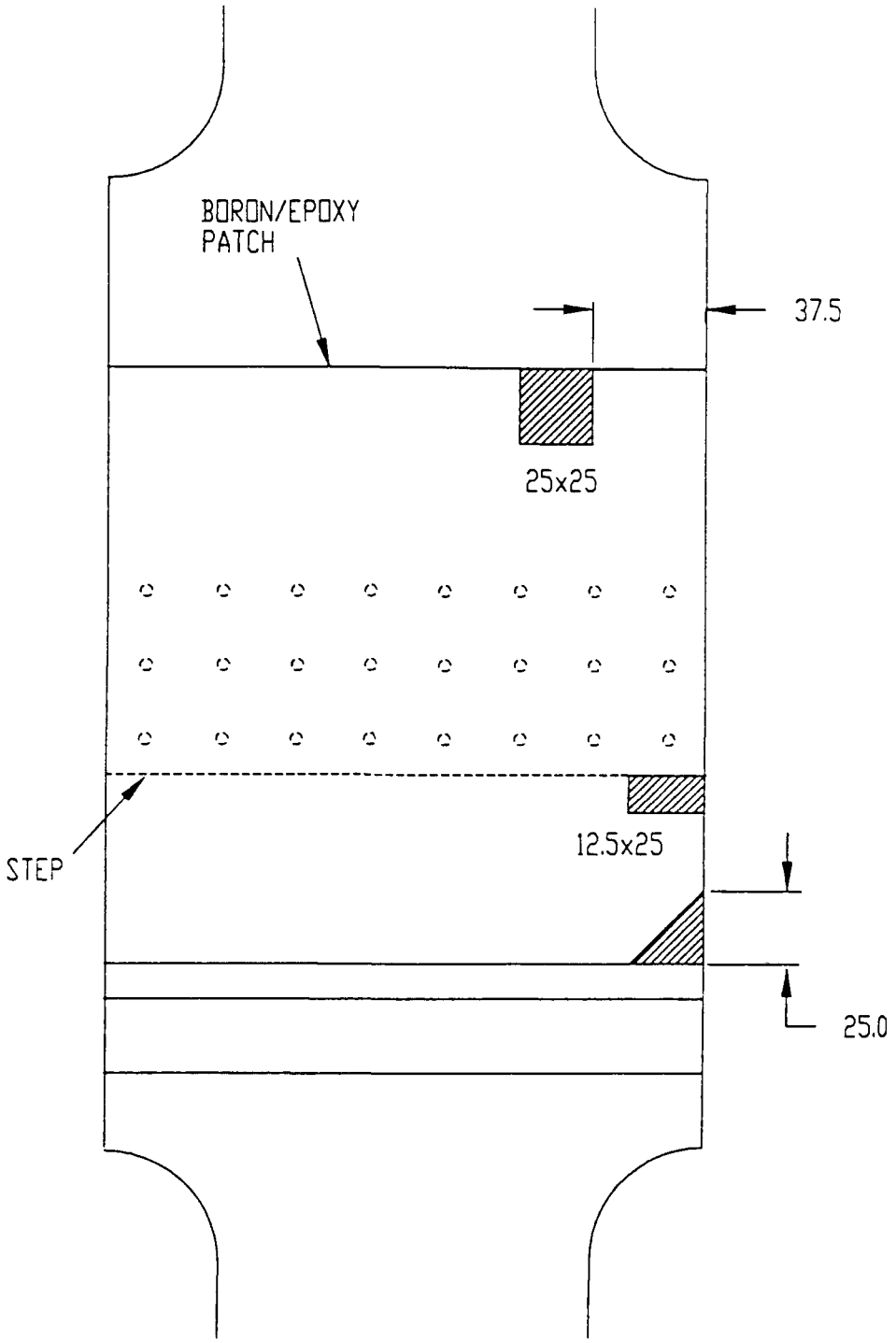

Figure 13: Insert detail for Specimen A6.

Figure 14: Specimen A9 with doubler removed.

Figure 15. Specimen A10 with doubler removed.

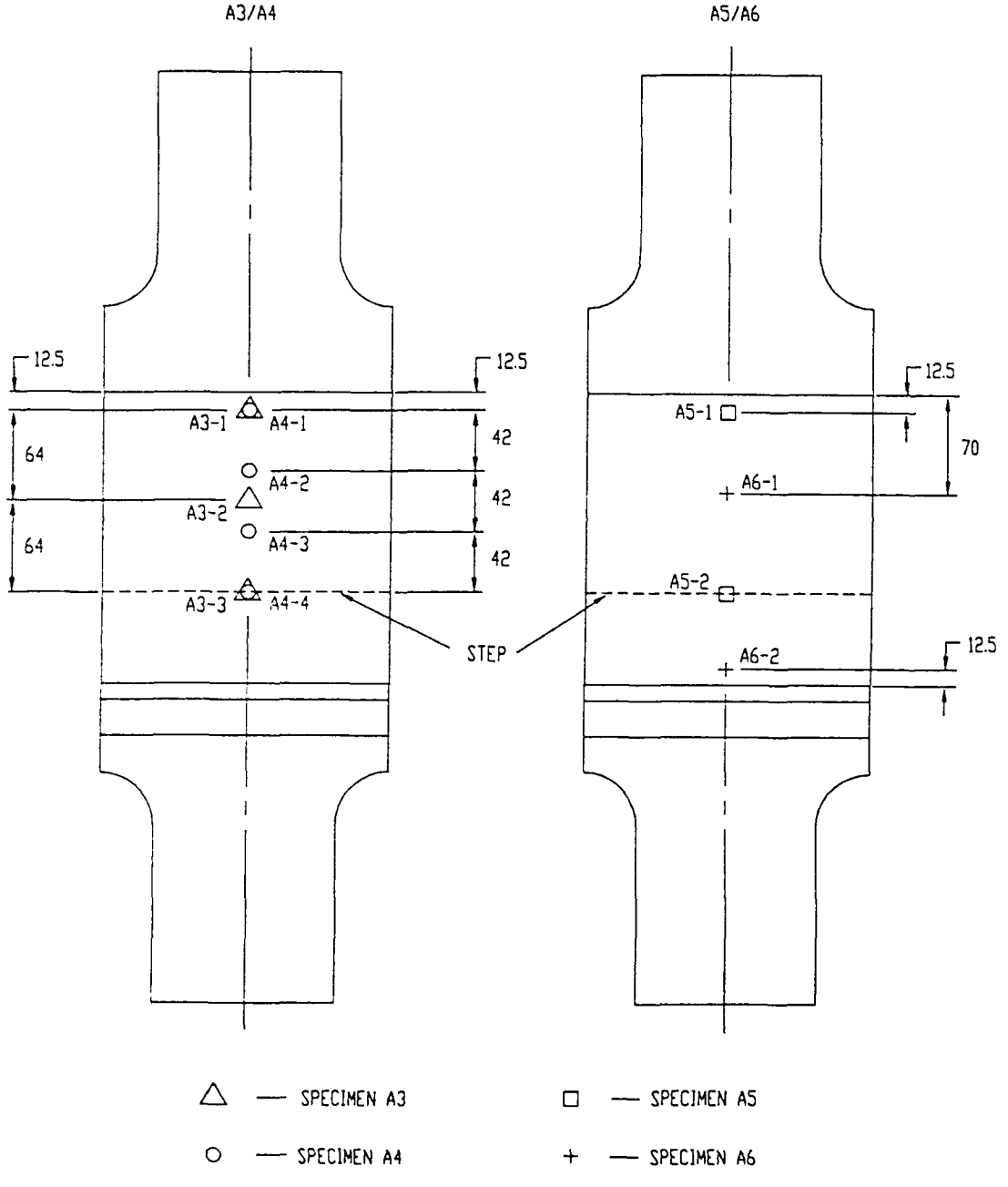

Figure 16: Impact site locations.

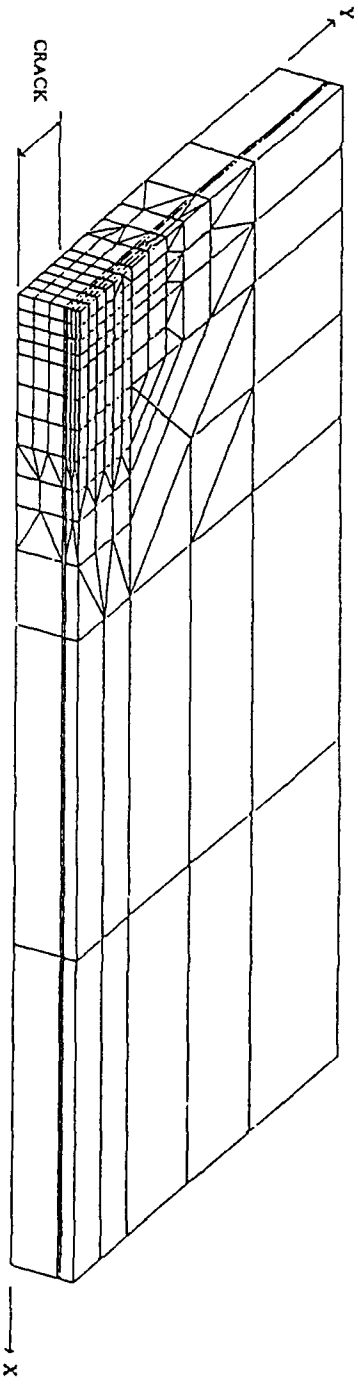

Figure 17: Mesh of 1/4 of the specimen.

DISTRIBUTION

AUSTRALIA

Department of Defence

Defence Central

Chief Defence Scientist
AS, Science Corporate Management } shared copy
FAS Science Policy
Director, Departmental Publications
Counsellor, Defence Science, London (Doc Data sheet only)
Counsellor, Defence Science, Washington (Doc Data sheet only)
Scientific Adviser, Defence Central
OIC TRS, Defence Central Library
Document Exchange Centre, DSTIC (8 copies)
Defence Intelligence Organisation
Librarian H Block, Victoria Barracks, Melb (Doc Data sheet only)

Aeronautical Research Laboratory

Director
Library
Chief of Airframes and Engines Division
Author: W.K. Chiu
D. Rees
P. Chalkley
R. Jones
M. Heller
R. Kaye

Navy Office

Navy Scientific Adviser (3 copies Doc Data sheet only)

Army Office

Scientific Adviser - Army (Doc Data sheet only)

Air Force Office

Air Force Scientific Adviser (Doc Data sheet only)
OIC ATF (2 copies)

SPARES (6 COPIES)

TOTAL (30 COPIES)

AL 149 DEPARTMENT OF DEFENCE

DOCUMENT CONTROL DATA

PAGE CLASSIFICATION
UNCLASSIFIED

PRIVACY MARKING

1a. AR NUMBER	1b. ESTABLISHMENT NUMBER	2. DOCUMENT DATE	3. TASK NUMBER
AR-007-070	ARL-STRUC-R-448	OCTOBER 1992	DST 92/069

4. TITLE
DESIGNING FOR DAMAGE TOLERANT COMPOSITE REPAIRS

5. SECURITY CLASSIFICATION (PLACE APPROPRIATE CLASSIFICATION IN BOX(S) IE. SECRET (S), CONF. (C) RESTRICTED (R), LIMITED (L) UNCLASSIFIED (U)).

DOCUMENT	TITLE	ABSTRACT
U	U	U

6. NO. PAGES
39

7. NO. REFS.
27

8. AUTHOR(S)
W.K. CHIU
D. REES
P. CHALKLEY
R. JONES

9. DOWNGRADING/DELIMITING INSTRUCTIONS
Not applicable.

10. CORPORATE AUTHOR AND ADDRESS
AERONAUTICAL RESEARCH LABORATORY
506 LORIMER STREET
FISHERMENS BEND VIC 3207

11. OFFICE/POSITION RESPONSIBLE FOR:
SPONSOR DSTO
SECURITY -
DOWNGRADING -
APPROVAL CAED

12. SECONDARY DISTRIBUTION (OF THIS DOCUMENT)

Approved for public release.

OVERSEAS ENQUIRIES OUTSIDE STATED LIMITATIONS SHOULD BE REFERRED THROUGH DSTIC, ADMINISTRATIVE SERVICES BRANCH, DEPARTMENT OF DEFENCE, ANZAC PARK WEST OFFICES, ACT 2601

13a. THIS DOCUMENT MAY BE ANNOUNCED IN CATALOGUES AND AWARENESS SERVICES AVAILABLE TO . . . .

No limitations.

13b. CITATION FOR OTHER PURPOSES (IE. CASUAL ANNOUNCEMENT) MAY BE [X] UNRESTRICTED OR [ ] AS FOR 13a.

14. DESCRIPTORS
Bonded composite repairs
Damage tolerance

15. DISCAT SUBJECT CATEGORIES
2011
1104

16. ABSTRACT

This paper presents a design methodology, and the associated data base, for the damage tolerant design of adhesively bonded repairs. This methodology is illustrated by considering repairs to an edge cracked panel and to multi-site damage in a fuselage lap joint.

PAGE CLASSIFICATION
UNCLASSIFIED
PRIVACY MARKING

THIS PAGE IS TO BE USED TO RECORD INFORMATION WHICH IS REQUIRED BY THE ESTABLISHMENT FOR ITS OWN USE BUT WHICH WILL NOT BE ADDED TO THE DISTIS DATA UNLESS SPECIFICALLY REQUESTED.

16. ABSTRACT (CONT).

17. IMPRINT

AERONAUTICAL RESEARCH LABORATORY, MELBOURNE

18. DOCUMENT SERIES AND NUMBER	19. COST CODE	20. TYPE OF REPORT AND PERIOD COVERED
Aircraft Structures Report 448	21 227C	

21. COMPUTER PROGRAMS USED

22. ESTABLISHMENT FILE REF.(S)

23. ADDITIONAL INFORMATION (AS REQUIRED)